



January 2015

Characterization Of Newly Synthesized Cobalt Polypyridine Complexes Using NMR, X-Ray, Electrochemistry, And UV-Vis

Blaise Frenzel

[How does access to this work benefit you? Let us know!](#)

Follow this and additional works at: <https://commons.und.edu/theses>

Recommended Citation

Frenzel, Blaise, "Characterization Of Newly Synthesized Cobalt Polypyridine Complexes Using NMR, X-Ray, Electrochemistry, And UV-Vis" (2015). *Theses and Dissertations*. 1771.
<https://commons.und.edu/theses/1771>

This Thesis is brought to you for free and open access by the Theses, Dissertations, and Senior Projects at UND Scholarly Commons. It has been accepted for inclusion in Theses and Dissertations by an authorized administrator of UND Scholarly Commons. For more information, please contact und.common@library.und.edu.

CHARACTERIZATION OF NEWLY SYNTHESIZED COBALT POLYPYRIDINE
COMPLEXES USING NMR, X-RAY, ELECTROCHEMISTRY, AND UV-VIS

by

Blaise Frenzel

Bachelor of Science, Bemidji State University, United States of America, 2011

A Thesis

Submitted to the Graduate Faculty

of the

University of North Dakota

in partial fulfillment requirements

for the degree of

Master of Science

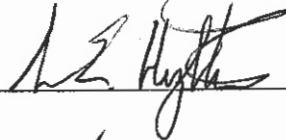
Grand Forks, North Dakota

May

2015

Copyright 2015 Blaise Frenzel

This thesis, submitted by Blaise Frenzel in partial fulfillment of the requirements for the Degree of Master of Science from the University of North Dakota, has been read by the Faculty Advisory Committee under whom the work has been done and is hereby approved.



Name of Chairperson



Name of Committee Member

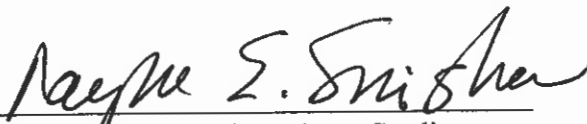


Name of Committee Member

Name of Committee Member

Name of Committee Member

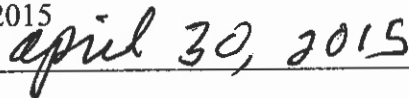
This thesis is being submitted by the appointed advisory committee as having met all of the requirements of the School of Graduate Studies at the University of North Dakota and is hereby approved.



Dean of the School of Graduate Studies

04/30/2015

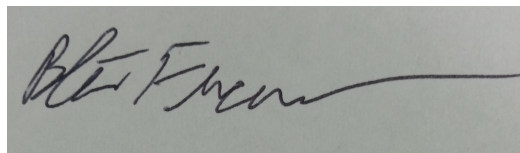
Date



PERMISSION

Title Characterization of Newly Synthesized Cobalt Polypyridine Complexes Using
NMR, X-Ray, Electrochemistry, and UV-vis.
Department Chemistry
Degree Master of Science

In presenting this thesis in partial fulfillment of the requirements for a graduate degree from the University of North Dakota, I agree that the library of this University shall make it freely available for inspection. I further agree that permission for extensive copying for scholarly purposes may be granted by the professor who supervised my thesis work or, in his absence, by the Chairperson of the department or the dean of the School of Graduate Studies. It is understood that any copying or publication or other use of this thesis or part thereof for financial gain shall not be allowed without my written permission. It is also understood that due recognition shall be given to me and to the University of North Dakota in any scholarly use which may be made of any material in my thesis.



Blaise Frenzel
Signature

04/30/15
Date

TABLE OF CONTENTS

LIST OF FIGURES	viii
LIST OF TABLE	x
ABSTRACT	xi
1. INTRODUCTION.....	1
1.1 A Brief History	1
1.2 Homoleptic Complexes.....	2
1.3 Heteroleptic Complexes	3
1.4 Statement of Purpose	4

2. HOMOLEPTIC COMPLEXES.....	5
2.1. General remarks	5
2.2. Physical measurements.....	5
2.3. Computational methods.....	6
2.4. Synthesis of the Homoleptic Compounds.....	7
2.4.1. <i>Synthesis of [Co(mer-bqp-κ³N,N',N'')₂](PF₆)₂</i>	7
2.4.2. <i>Synthesis of [Co(mer-bqp-κ³N,N',N'')₂][Br₃]₃</i>	8
2.4.3 <i>X-ray crystallography</i>	8
2.5. Results and Discussion For Homoleptic Cobalt Complexes	9
2.5.1 <i>Ligand Synthesis</i>	9
2.5.1 <i>X-ray crystal structure analysis</i>	12
2.5.2. <i>Magnetic susceptibility</i>	18
2.5.3 <i>Electronic spectra</i>	19
2.5.4 <i>Electrochemistry</i>	24

3. HETEROLEPTIC COMPLEXES	26
3.1. General remarks	26
3.2. Physical measurements	26
3.3. Synthesis of Heteroleptic Complexes	27
3.3.1 <i>Synthesis of Co(mer-bqp-κ³N,N',N'')(bpy-κ²N,N')Cl][PF₆]₂ (5)</i>	28
3.3.2 <i>Synthesis of Co(mer-tpy-κ³N,N',N'')(phen- κ²N,N')Cl][PF₆]₂ (3)</i> <i>and Co(mer-tpy-κ³N,N',N'')(bpy-κ²N,N')Cl][PF₆]₂ (4)</i>	28
3.4 Characterization of [Co(mer-tpy-κ ³ N,N',N'')(phen- κ ² N,N')Cl][PF ₆] ₂	30
3.4.1. <i>Ligand Synthesis</i>	30
3.4.2. <i>X-Ray Crystallography</i>	30
3.4.3. <i>NMR Spectroscopy</i>	32
3.4.4. <i>Electrochemistry</i>	37
4. CONCLUSION	41
APPENDIX	44
REFERENCES	69

LIST OF FIGURES

Figure	Page
1. Thermal ellipsoid view of mer,mer-[Co(bqp-κ ₃ N,N',N'') ₂] ²⁺ (1).....	10
2. Thermal ellipsoid view of mer,mer-[Co(bqp-κ ³ N,N',N'') ₂] ³⁺ (2).....	11
3. DFT (B3LYP/LANL2DZ) optimized structures of high-spin mer,mer-[Co(bqp-κ ₃ N,N',N'') ₂] ²⁺	17
4. Absorption spectra for mer,mer-[Co(bqpκ ₃ N,N',N'') ₂] ²⁺ (1 ; black, short dash) and mer,mer-[Co(bqp-κ ₃ N,N',N'') ₂] ³⁺ (2 ; black, solid line) in acetonitrile at room temperature.....	20
5. Comparison of molecular orbitals for mer,mer-[Co(bqp-κ ₃ N,N',N'') ₂] ³⁺ (2).	22
6. Simulated absorption spectrum for mer,mer-[Co(bqp- κ ₃ N,N',N'') ₂] ³⁺ (2)	23
7. Cyclic voltammograms for mer,mer-[Co(bqp-κ ₃ N,N',N'') ₂] ³⁺ (2 , top) and mer,mer-[Co(bqp-κ ₃ N,N',N'') ₂] ²⁺ (1 , bottom).....	24
8. Solid-state structure of [Co(mer-tpy- κ ₃ N,N',N'')(phen-κ ₂ N,N',N'')Cl][PF ₆] ₂	28
9. [Co(mer-tpy-κ ₃ N,N',N'')(phen- κ ₂ N,N')Cl][PF ₆] ₂	32
10. Spectra of [Co(mer-tpy-κ ³ N,N',N'')(phen-κ ² N,N')Cl] ₂	33
11. Marked [Co(mer-bqp-κ ³ N,N',N'')(bpy-κ ² N,N')Cl][Br ₃] ₂	34
12. Spectra of [Co(mer-bqp-κ ³ N,N',N'')(bpy-κ ² N,N')Cl] ₂	34
13. Selected voltammograms for [Co(mer-tpy-κ ³ N,N',N'')(bpy-κ ² N,N')Cl][PF ₆] ₂ , top, and [Co(mer-tpy-κ ³ N,N',N'')(phen-κ ² N,N')Cl][PF ₆] ₂ , bottom.....	37
14. Selected voltammogram for [Co(mer-bqp-κ ³ N,N',N'')(bpy-κ ² N,N')Cl][Br ₃] ₂	38
15. Selected voltammogram for the oxidation and second reduction of [Co(mer-bqp-κ ₃ N,N',N'')(bpy-κ ² N,N')Cl][Br ₃] ₂	39
16. S1- Cobalt-Bis(8'-quinolinyl)pyridine (bqp) Geometries.....	66

17. S2-Cobalt-Bis(8'-quinoliny)pyridine (bqp) Configurations.....	67
18. S3-Overlay of the x-ray structures at 100 and 290 K for [Co(<i>mer</i> -bqp- κ^3N,N',N'')) ₂]... ..	68

LIST OF TABLES

Table	Page
1. Selected bond lengths [Å] and angles [°] for <i>mer,mer</i> -[Co(bqp-κ ³ N,N',N'')) ₂] ²⁺ [1].	12
2. Selected bond lengths [Å] and angles [°] for <i>mer,mer</i> -[Co(bqp-κ ³ N,N',N'')) ₂] ³⁺ [2].	14
3. Electronic absorption maxima.....	21
4. Selected bond lengths and angles for [Co(<i>mer</i> -tpy-κ ² N,N',N''))(phen-κ ² N,N',N''))] ²⁺ .	30
5. Selected bond lengths and angles for [Co(<i>mer</i> -tpy-κ ² N,N',N''))(bpy-κ ² N,N',N''))] ²⁺ .	31
6. Table S1. Selected bond length [Å] and angles [°] for [Co(<i>mer</i> -tpy-κ ³ N,N',N'')) ₂] ²⁺ and [Co(<i>mer</i> -tpy-κ ³ N,N',N'')) ₂] ³⁺	46
7. Table S2. DFT Calculations. Selected bond length [Å] and angles [°] for [Co(<i>mer</i> -bqp-κ ³ N,N',N'')) ₂] ²⁺ (low and high spin) and [Co(<i>mer</i> -bqp-κ ³ N,N',N'')) ₂] ³⁺ ..	47
8. Table S3-A. Optimized Geometry [Co(<i>mer</i> -bqp-κ ³ N,N',N'')) ₂] ²⁺ (1) in the Doublet Ground State with E(B3LYP) = -2244.39629091 au.....	48
9. Table S3-B. Calculated doublet excited states of for [Co(<i>mer</i> -bqp-κ ³ N,N',N'')) ₂] ²⁺ (1) in acetonitrile (CH ₃ CN).....	50
10. Table S3-C. Fragment Analysis Based on Mullikan Populations for Co(<i>mer</i> -bqp-κ ³ N,N',N'')) ₂] ²⁺ (1) in the Doublet Ground State (Alpha-Spin).....	54
11. Table S3-D. Fragment Analysis Based on Mullikan Populations for [Co(<i>mer</i> -bqp-κ ³ N,N',N'')) ₂] ²⁺ (1) in the Doublet Ground State (Beta-Spin).....	56
12. Table S4-A. Optimized Geometry of [Co(<i>mer</i> -bqp-κ ³ N,N',N'')) ₂] ³⁺ (2) in the Singlet Ground State with E(B3LYP) = -2244.20766539 au.....	58
13. Table S4-B. Calculated singlet excited states of for [Co(<i>mer</i> -bqp-κ ³ N,N',N'')) ₂] ³⁺ (2) in acetonitrile (CH ₃ CN).....	60
14. Table S3-C. Calculated triplet excited states of for [Co(<i>mer</i> -bqp-κ ³ N,N',N'')) ₂] ³⁺ (2) in acetonitrile (CH ₃ CN).....	63
15. Table S4-D. Fragment Analysis Based on Mullikan Populations for - [Co(<i>mer</i> -bqp-κ ³ N,N',N'')) ₂] ³⁺ (2) in the Singlet Ground State.....	64

ABSTRACT

Coordination of the 2,6-bis(8'-quinolinyl)pyridine (**bqp**) ligand to a cobalt (Co) core and its influence to electron spin and configuration on the structures and properties of the resulting complexes has been investigated. The homoleptic complexes [Co(*mer*-**bqp**- κ^3N,N',N'')₂][PF₆]₂ (**1**) and [Co(*mer*-**bqp**- κ^3N,N',N'')₂][Br₃]₃ (**2**) were prepared and characterized. X-ray structure determinations of complexes **1** and **2** revealed twisted, near-octahedral arrangements relative to the cobalt center. The magnetic data for **1** is typical of those for distorted octahedral (i.e., *D*_{4h} symmetry) high-spin d⁷ species despite the near-ideal octahedral coordination of the **bqp** ligand around the Co(II) core. Electronic spectra for **1** and **2** have been investigated and assigned. Both complexes exhibit intense π - π^* **bqp** ligand centered transitions in the UV region and low intensity mixed charge transfer transitions in the visible region. Neither complex strongly absorbs in visible spectral region. The electrochemistry of these compounds has been studied and compared to that of similar cobalt terpyridine compounds. A metal-centered Co^{2+/3+} redox wave and ligand-based reduction processes were observed for **1** and **2** in acetonitrile. The metal-centered redox potentials were reversible with potentials more positive than comparable cobalt-terpyridine complexes. Density functional theory (DFT) calculations of the electronic and ground state properties are in good agreement with the experimental data.

CHAPTER 1

1. INTRODUCTION

1.1 A Brief History

The first reported transition metal terpyridine complex was developed by Morgan and Burstall in the 1930s. The complex was synthesized using iron and 2,2':6',2''-terpyridine (**tpy**), which produced $[\text{Fe}(\text{tpy})_2]^{2+}$.^{1,2} Since then there have been a tremendous amount of studies looking into using these complexes that have polypyridine ligands attached to transition metals. Currently, these polypyridine ligands, bound with early transition metals and actinide metals, have been investigated thoroughly. As a result, there is reason/precedent to synthesize and research late transition metal complexes, particularly those of d^6 , d^8 , and d^{10} groups. The stability and rich photophysical and electrochemical properties for many polypyridine complexes have been evolving into applications in emerging fields of catalysis, optoelectronics, and life sciences.

One example is $[\text{Ru}(4,4',4''\text{-(COOH)}_3\text{-terpy})(\text{NCS})_3]$, also known as the “black dye,” as a sensitizer in dye-sensitized solar cells (DSSCs)³. Another example would be that of $[\text{Pt}(\text{tpy})\text{Cl}][\text{Cl}]$ as a potent anti-tumor drug that attacks malignant cancers. A complete study of these complexes would be beyond the work of this thesis. Herein will be described the findings of both homoleptic and heteroleptic complexes.

1.2 Homoleptic Complexes

Multi-dentate polypyridine ligands, such as 2,2':6',2''-terpyridine (**tpy**), 2,2'-bipyridine (**bpy**), and 1,10-phenanthroline (**phen**), are attractive ligands for constructing various catalytic, photo- and redox-active structures.^{5a} Among these, tridentate terpyridine derivatives are particularly unique from the viewpoint of synthetic and structural coordination chemistry⁶. Synthetic modification of the 4'-site on the **tpy** ligand is attractive as it does not result in isomeric complexes due to the existence of a twofold axis of symmetry in the **tpy**- κ^3N,N',N'' chelate^{2c}. This leads to the formation of well-defined structures where directionality is desirable, such as surface attachment and polymerization applications^{5,6,7}. Because of their planar nature, terpyridine derivatives coordinate almost exclusively as meridional tridentate ligands, and structural changes are restricted when the oxidation state of the center changes^{2c}. In this context, bis(terpyridine) metal complexes of the type $[M(\mathbf{tpy})_2]X_2$ (**tpy** = 2,2';6',2''-terpyridine; X^- is, commonly, Cl^- , ClO_4^- , or PF_6^-) have been widely investigated due to their inert character and catalytic activity applied to the fields of light-into-energy conversion⁸ and artificial photosynthesis⁹. Recently, materials have even been developed based on bis(terpyridine) cobalt(II) spin crossover systems¹⁰.

Recently, researchers have used 2,6-bis(8'-quinolinyl)pyridine (**bqp**) ligand to produce homoleptic six-membered chelate rings instead of the traditional five-membered metallocycle rings formed in $[M(\mathbf{tpy})_2]X_2$ complexes¹¹. The result of this design is to optimize the N–M–N intraligand and bite angles towards idealized octahedral values of 90° and 180°, respectively, and thereby strengthening the ligand field¹¹. This strategic

design has led to improved quantum yields and prolonged excited state triplet lifetimes for the $[\text{Ru}(\text{tpy})_2]^{2+}$ complexes. Johansson and co-workers showed that when coordinated to a Ru^{II} center, the **bqp** ligand's bite angles were increased and its steric strain reduced, compared to normal terpyridines^{11,12}. As a result, the Ru^{II} bistridentate **bqp** complex exhibited significantly increased emission lifetimes due to a stronger ligand field and a lower rate of population of the ^3MC state^{6,11}.

1.3 Heteroleptic Complexes

Polypyridine ligands are particularly attractive for constructing various catalytic, photo- and redox-active structures.⁵ Among those ligands 2,2':6',2''-terpyridine (**tpy**) and 2,6-bis(8'-quinolinyl)pyridine (**bqp**) are particularly unique because of their planar nature, which results in meridional tridentate coordination. Because of this unique coordination, an effective use of these ligands is to combine them with bidentate auxiliary ligands such as 2,2'-bipyridine (**bpy**), and 1,10-phenanthroline (**phen**) and developing mixed ligand (heteroleptic) complexes.

These mixed ligand terpyridine complexes have been synthesized previously by utilizing various 4d and 5d metal ions such as ruthenium, rhodium, osmium, and iridium¹³. However, these metals are rare and costly; therefore, more abundant transition metals are desirable. As such, the 3d metal cobalt would be an attractive alternative. Unfortunately, 3d metal complexes are significantly more difficult to isolate because of the high tendency for ligand substitution.

Even though these complexes are difficult to prepare and isolate, research concerning heterolytic complexes is still promising. Complexes of the type $[\text{M}(\text{tpy}/\text{bqp})$

(**bpy/phen**)X]ⁿ⁺ (X being a halogen) are valuable. These complexes have mixed ligands which employ either the **tpy** or **bqp** as the tridentate ligand and use an auxiliary bidentate ligand, such as **bpy** or **phen**. The remaining site is occupied by a halide ligand which can be removed in a straightforward manner. This, in essence, leaves a “vacant” site. This vacant octahedral coordination site can then be utilized as a site for catalytic reactions.

1.4 Statement of Purpose

This thesis describes the synthesis, structural, spin state and electronic properties of two homoleptic bis(2,6-bis(8'-quinolinyl)pyridine) cobalt complexes [Co(*mer*-**bqp**-κ³N,N',N'')][PF₆]₂ (**1**) and [Co(*mer*-**bqp**-κ³N,N',N'')][Br₃]₃ (**2**) which differ only in the oxidation state of the central metal. Also described are three heteroleptic species including [Co(*mer*-**tpy**-κ³N,N',N'')(**phen**-κ³N,N')Cl][PF₆]₂ (**3**), [Co(*mer*-**tpy**-κ³N,N',N'')(**bpy**-κ³N,N')Cl][PF₆]₂ (**4**), and [Co(*mer*-**bqp**-κ³N,N',N'')(**phen**-κ³N,N')Cl][Br₃]₂ (**5**). Spectroscopic, magnetic and electrochemical properties of the compounds are obtained, and crystal structures of them, are discussed. Coordination of the **bqp** ligand was expected to change the ligand bite angles to near-ideal octahedral symmetries as well as the stability, flexibility, electronic and redox behavior of the resulting complexes. These features of ligand coordination can potentially play a role in the stabilization (or destabilization) of particular spin states, electronic states, or redox states in the resulting complexes, providing valuable information for further developments, in particular for the design of ligands capable of generating mixed-spin states, mixed-valent multi-nuclear compounds or redox mediators in dye-sensitized solar cells.

CHAPTER 2

2. HOMOLEPTIC COMPLEXES

2.1. General remarks

Cobalt(II) acetate tetrahydrate, $\text{Co}(\text{CH}_3\text{COO})_2 \cdot 4\text{H}_2\text{O}$, ammonium hexafluorophosphate (NH_4PF_6) and bromine (Br_2) were purchased from Aldrich and used without further purification. The 2,6-bis(8'-quinolinyl)pyridine (**bqp**) ligand was prepared in accordance to a previous literature report¹².

All solvents for synthesis were of reagent grade and used as received, unless otherwise specified. Anhydrous methanol (CH_3OH) and acetonitrile (CH_3CN) were distilled from Na/benzophenone⁹. For UV-vis spectroscopy and electrochemical studies HPLC grade or reagent grade solvents were used. The reagent grade acetonitrile was first dried over silica gel for a minimum of 24 h. The silica gel was then filtered off and the acetonitrile was distilled over anhydrous calcium hydride¹⁴.

2.2. Physical measurements

UV/vis spectra were recorded using a Cary 50 UV-vis spectrophotometer with a xenon flashlamp. Room temperature emission spectra were measured on a Cary Eclipse fluorescence spectrophotometer. Low temperature excitation and emission spectra were obtained with a Photon Technologies International QuantaMaster Model C-60 spectrometer equipped with a xenon flash lamp and digital emission photon multiplier tube using a band pathway of 5 nm for excitation and 2 nm for emission. Voltammetry of the complexes was measured using acetonitrile as the solvent and tetra-*n*-butylammonium

hexafluorophosphate (TBAPF₆, 0.1 M) as the supporting electrolyte. The electrolyte was recrystallized in absolute ethanol and dried under vacuum in a desiccator for a minimum of 24 h prior to use¹⁵. Cyclic voltammograms were recorded using a PINE WaveNow potentiostatic analyzer in a three-electrode configuration. A glassy-carbon disk working electrode (3 mm diameter), a non-aqueous Ag⁺/AgCl wire quasi-reference electrode, and a Pt disk counter electrode were used for all measurements. Recorded potentials were referenced using the ferrocene/ferrocenium couple (vs. SCE) as an internal standard usually added at the conclusion of the experiment¹⁶. ¹H and ¹³C NMR spectra were measured with a Bruker AVANCE 500 high-field superconducting NMR spectrometer. Electrospray ionization (ESI) mass spectra were obtained with an Agilent Time-of-Flight MS G1969A Series 6200 in positive ionization mode using 1 ppm of the complexes in a 50% acetonitrile/water (LC/MS) with 10 μM of acetic acid (ionization agent). Magnetic susceptibility measurements in the solid state were carried out on a Johnson Matthey Mark 1 magnetic susceptibility balance. Elemental analyses were performed by Atlantic Microlab, Inc., Norcross, GA.

2.3. Computational methods

DFT calculations were carried out by using Gaussian 09, revision A.02¹⁷. For Gaussian calculations, Becke's three-parameter hybrid functional with the LYP correlation functional (B3LYP)¹⁸ was used with the Los Alamos effective core potential LANL2DZ¹⁹ basis set. Full geometry optimizations were performed using the B3LYP functional¹⁸. A double- ζ quality basis set consisting of Hay and Wadt's effective core potentials (LANL2DZ)¹⁹ was employed for the Co(II and III) metal ions, and a

6-31G* basis set²⁰ was employed for the rest of the atoms. The relativistic effective core potential (ECP) replaced the inner core electrons of the Co(II and III) metal ions, leaving only the outer core valence electrons (4s²4p⁶3d⁷ and 4s²4p⁶3d⁶ for Co(II) and Co(III), respectively). A vibrational frequency analysis was carried out in order to confirm the minimum-energy geometries. Molecular orbital (MO) diagrams were constructed for the fully optimized geometries in Gaussian. The Franck–Condon vertical excitation energies and oscillator strengths were obtained with time-dependent DFT (TD-DFT)²¹ as implemented in Gaussian. The acetonitrile solvent influence was treated using conductor-like polarizable continuum model (CPCM)²², as implemented in Gaussian.

2.4. Synthesis of the Homoleptic Compounds

2.4.1. Synthesis of [Co(*mer*-bqp- κ^3 N,N',N'')₂](PF₆)₂

2,6-Bis(8'-quinoliny)pyridine (0.05 g, 1.5 × 10⁻⁴ mol) was added to an anhydrous methanol solution (30 mL) containing cobalt(II) acetate tetrahydrate (0.018 g, 7.2 × 10⁻⁵ mol). Once addition was complete, the reaction was stirred at room temperature for 2 h. Once stirring was complete, an excess of ammonium hexafluorophosphate (1.0 g, 6.1 × 10⁻³ mol) was added and immediate precipitation was observed. This was followed by the addition of water (distilled, 20 mL). The resulting brown precipitate was filtered, washed with cold water (3 × 10 mL) and diethyl ether (3 × 10 mL), and dried under vacuum. Yield: 93%. *Anal.* Calc. for C₄₆H₃₀CoF₁₂N₆P₂: C, 54.29; H, 3.17; N, 8.26. Found: C, 53.86; H, 3.15; N, 8.25%. Electronic absorption (CH₃CN), λ_{\max} , nm (ϵ , M⁻¹ cm⁻¹): 203 (102374, sh.), 225 (85775), 282 (21152), 306 (19929), 315 (19521), 360 (5522), 460 (1076, br.). ESI MS: m/z 363 (parent peak, [M], where M is [Co(*mer*-bqp- κ^3 N,N',N'')₂]²⁺).

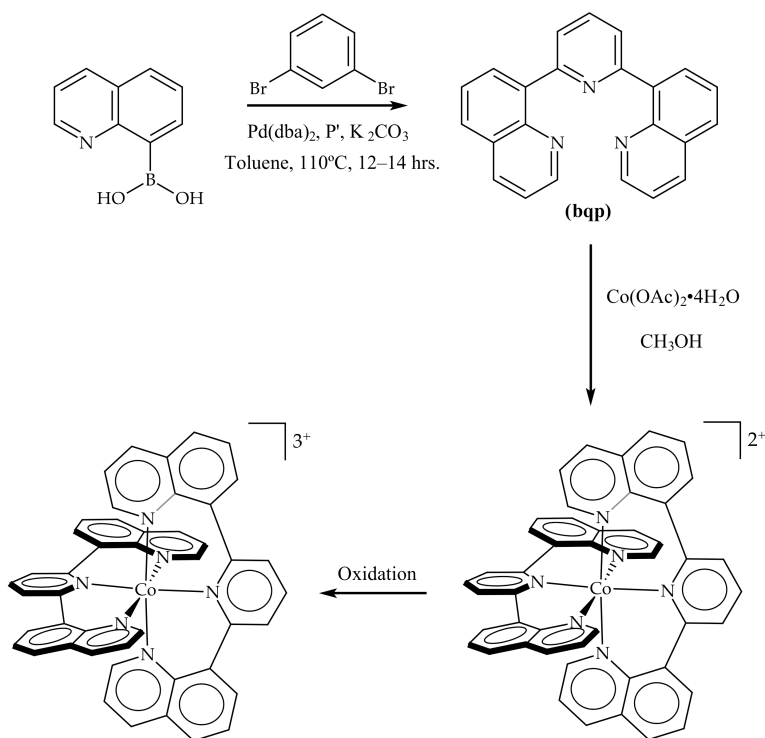
2.4.2. Synthesis of $[\text{Co}(\text{mer-bqp-}\kappa^3\text{N,N',N''})_2][\text{Br}_3]_3$

Bromine (0.100 g, 1.25×10^{-3} mol) was added to a stirred solution of $[\text{Co}(\text{mer-bqp-}\kappa^3\text{N,N',N''})_2][\text{PF}_6]_2$ (0.068 g, 6.7×10^{-5} mol) and acetonitrile (20 mL). Once the addition was complete, the reaction was stirred at room temperature for 5 h. The resulting solution was evaporated to dryness under reduced pressure. The resulting dark orange solid was collected, washed with water (3×10 mL), and dried under vacuum. The yield was quantitative (0.079 g). ^1H NMR ($\text{CD}_3\text{CN-}d_3$): δ 8.50 (dd, $J = 8.0$ Hz, 2H), 8.45 (t, $J = 8.0$ Hz, 1H), 8.08 (m, 4H), 8.03 (dd, $J = 4.6$ Hz, 2H), 7.92 (dd, $J = 4.1$ Hz, 2H), 7.68 (t, $J = 8.0$ Hz, 2H), 7.42 (dd, $J = 8.1$ Hz, 2H). ^{13}C NMR ($\text{CD}_3\text{CN-}d_6$): δ 162.1, 154.5, 143.9, 143.3, 142.5, 133.2, 132.8, 129.7, 128.2, 128.0, 126.8, 124.1. *Anal.* Calc. for $\text{C}_{46}\text{H}_{30}\text{CoBr}_9\text{N}_6$: C, 43.11; H, 2.21; N, 11.17. Found: C, 42.59; H, 2.18; N, 11.09%. Electronic absorption (CH_3CN), λ_{max} , nm (ϵ , $\text{M}^{-1} \text{cm}^{-1}$): 208 (138612), 218 (131456, sh.), 266 (67709), 330 (28168, sh.), 357 (31095), 380 (19101, sh.), 461 (506, br.), 626 (0.1, br.). ESI MS: m/z 242 (parent peak, $[\text{M}]$, where M is $[\text{Co}(\text{mer-bqp-}\kappa^3\text{N,N',N''})_2]^{3+}$). Note: prior to electrochemical studies an excess of ammonium hexafluorophosphate (1.0 g, 6.1×10^{-3} mol) was added and immediate precipitation was observed. This was followed by the addition of water (distilled, 20 mL). The resulting orange precipitate was filtered, washed with cold water (3×10 mL) and diethyl ether (3×10 mL), and dried under vacuum.

2.4.3 X-ray crystallography

Crystals of the complexes suitable for X-ray crystallography were obtained through slow evaporation in acetonitrile. Intensity data for a brown crystal of $[\text{Co}(\text{mer-bqp-}\kappa^3\text{N,N',N''})_2][\text{PF}_6]_2$ and a dark orange crystal of $[\text{Co}(\text{mer-bqp-}\kappa^3\text{N,N',N''})_2][\text{Br}_3]_3$ were

measured at 100 K with a Bruker APEX-II CCD diffractometer fitted with graphite-monochromated Mo K α radiation (0.71073 Å). The data were collected to a maximum 2θ value of 22.3° and processed using the Bruker software. Both structures were solved by direct methods and expanded using standard Fourier routines in the SHELX-97 software package²³. All hydrogen atoms were placed in idealized positions, and all non-



Scheme 1. Synthetic routes for *mer,mer*-[Co(bqp- κ^3N,N',N'')₂]²⁺ (**1**) and *mer,mer*-[Co(bqp- κ^3N,N',N'')₂]³⁺ (**2**).

hydrogen atoms were refined anisotropically.

2.5. Results and Discussion For Homoleptic Cobalt Complexes

2.5.1 Ligand Synthesis

The 2,6-bis(8'-quinolinyl)pyridine (**bqp**) ligand was prepared by modification to the route first described by Hammarström et al.¹² using Suzuki cross-coupling reaction

conditions following the procedures developed by Buchwald and coworkers²⁴. For the Suzuki cross-coupling reaction, a catalytic system including palladium(0)

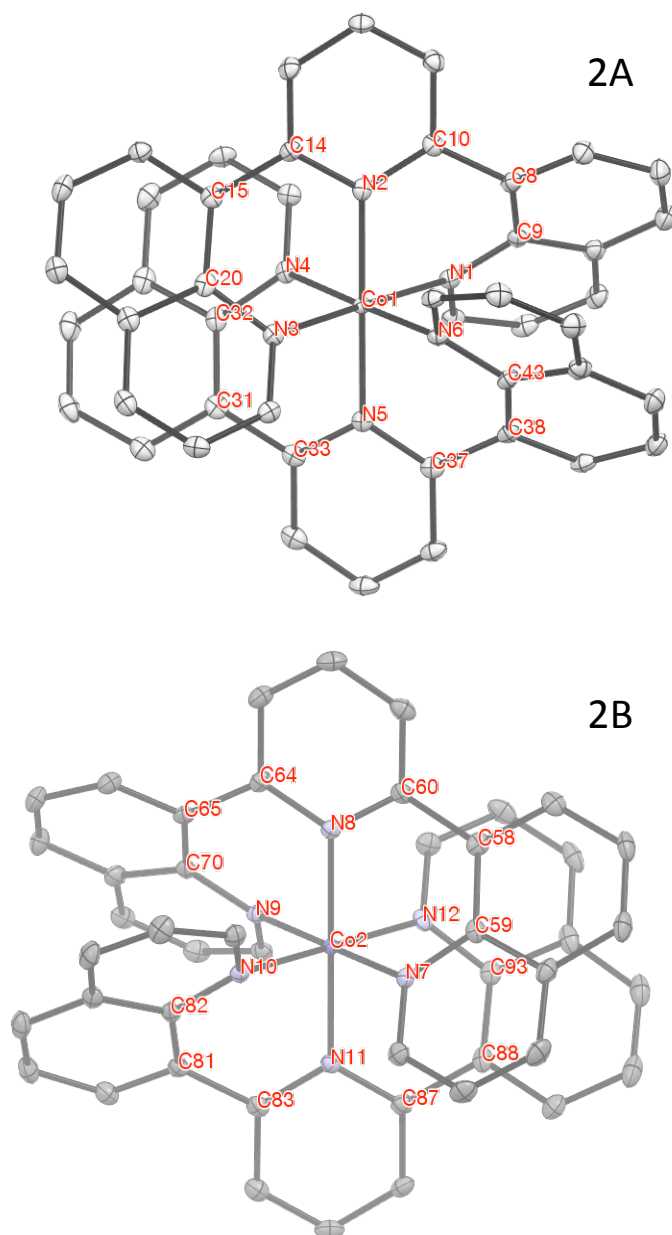


Figure 2. Thermal ellipsoid view of *mer,mer*-[Co(bqp- κ^3N,N',N'')₂]³⁺ (**2**) (50% probability, 100 K; H atoms omitted). Both crystallographic units shows as 2A and 2B respectively.

bis(dibenzylideneacetone) (Pd(dba)₂) and 2-dicyclohexylphosphino-2',6'-

dimethoxybiphenyl (P') was implemented, which recently has been effective in coupling heterocyclic substrates^{25,26}. Reacting quinoline-8-boronic acid and 2,6-dibromopyridine with 1 mol% of Pd(dba)₂ and 2 mol% of P' in toluene at 110 °C gave **bqp** in 80% isolated yield (Scheme 1).

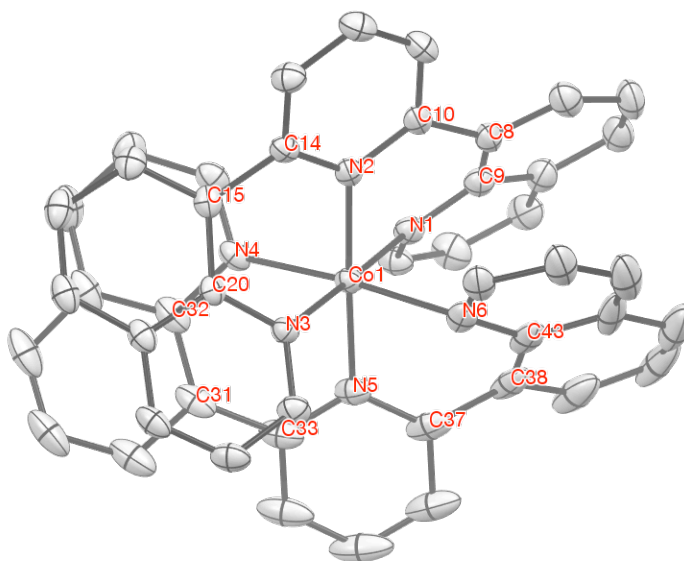


Figure 1. Thermal ellipsoid view of *mer,mer*-[Co(bqp- κ^3 N,N',N'')₂]²⁺ (**1**) (50% probability, 100 K; H atoms omitted).

Syntheses of the complexes were prepared in analogy to a previous literature report by Constable et al.²⁶. The homoleptic complex **1** was obtained by stirring a 1:2 mixture of Co(OAc)₂·4H₂O and the desired **bqp** ligand in deoxygenated, anhydrous methanol. The crude product was precipitated by addition of aqueous NH₄PF₆. The resulting brown precipitate was filtered, washed with cold water and diethyl ether. This one pot approach proved to be a very convenient, high-yielding (>93%) route for the preparation of **1**.

Oxidation of **1** was performed by adding Br₂ to a stirred solution of **1** and CH₃CN. The reaction was stirred at room temperature and the resulting solution was evaporated to dryness under a reduced pressure. The resulting dark orange solid **2** was collected, washed with water, and dried under vacuum. The yield was quantitative. The ¹H and ¹³C NMR spectra of complex **2** were assigned by careful examination of the integration and splitting patterns, as well as by comparison to similar Co(II)-terpyridine derivatives^{5c} and Ru(II)-**bqp**¹² complexes.

2.5.1 X-ray crystal structure analysis

Crystals of [Co(*mer*-**bqp**-κ³N,N',N'')₂][PF₆]₂ (**1**) and [Co(*mer*-**bqp**-κ³N,N',N'')₂][Br₃]₃ (**2**) were grown by slow evaporation in acetonitrile. Structural analyses for **1** and **2** reveals a twisted, near-octahedral arrangement relative to the cobalt center. The 2,6-bis(8'-quinolinyl)pyridine ligands are coordinated in a tridentate fashion and are meridionally arranged about the cobalt core with resultant **bqp** ligand coordination planes lying perpendicular to each other. No evidence for facial isomers was found. This stands in contrast to previous reports where coordination of **bqp** to a ruthenium(II) core produced both facial and meridional isomers¹². It stands to reason, the cobalt core allows

Table 1. Selected bond lengths [Å] and angles [°] for *mer,mer*-[Co(**bqp**-κ³N,N',N'')₂]²⁺ [**1**].

Co1–N1	2.000 (3)	Co1–N4	2.182 (3)
Co1–N2	1.936 (3)	Co1–N5	1.963 (3)
Co1–N3	2.011 (3)	Co1–N6	2.187 (3)
N2–Co1–N1	89.75 (11)	N5–Co1–N4	87.77 (12)
N2–Co1–N3	90.25 (11)	N5–Co1–N6	87.61 (13)

Table 1. Cont.

N1–Co1–N3	178.35 (12)	N4–Co1–N6	175.22 (11)
N2–Co1–N4	94.22 (11)	N5–Co1–N3	90.18 (11)
N2–Co1–N6	90.41 (11)	N5–Co1–N1	89.88 (11)
N2–Co1–N5	177.94 (13)	N3–Co1–N4	93.04 (10)
N1–Co1–N4	85.31 (11)	N3–Co1–N6	85.77 (11)
N1–Co1–N6	95.88 (11)		
N2–C10–C8–C9	27.7 (5)	N5–C33–C31–C32	39.3 (5)
N2–C14–C15–C20	43.5 (5)	N5–C37–C38–C43	41.4 (5)

the **bqp** ligand to optimally orientate upon coordination resulting in the meridional arrangement.

The X-ray crystal structure for the dication of $[\text{Co}(\text{mer-}\mathbf{bqp}\text{-}\kappa^3\text{N},\text{N}',\text{N}'')_2][\text{PF}_6]_2$ is shown in (Fig. 1), with selected bonds lengths and angles given in Table 1. The **bqp** ligands occupy different environments around the Co(II) core. As a result, two complementary dihedral angles of approximately 39° and 41° (for one **bqp** ligand) and 28° and 44° (for the second **bqp** ligand) exist between the quinolines (Qn) and central pyridine (Py) ring systems. All N–Co–N intraligand angles are near 90° . The bite angles between the ligands are 178° and 175° , respectively, which are indicative of the non-equivalent coordination environment around the Co(II) metal. As has been noted for complexes with tridentate terpyridine ligands of this kind with first row metal atoms²⁷, there is considerable tetragonal compression: the Co–N_{Py} bond length being on average $\sim 1.946 \text{ \AA}$, which is shorter than the Co–N_{Qn} bond lengths by . As a result, the point group symmetry of **1** is lowered to pseudo D_{4h} .

In contrast, the high-spin case for a tetragonally compressed d^7 metal center of D_{4h} symmetry ($b_{2g}^2 e_g^3 b_{1g}^1 a_{1g}^1$) should only experience weak Jahn–Teller distortion while the ligand strain of the tridentate ligand should still be active²⁸. As a result, the

Table 2. Selected bond lengths [Å] and angles [°] for *mer,mer*-[Co(bqp- κ^3N,N',N'')₂]³⁺ [2].

2A			
Co1–N1	1.956 (2)	Co1–N4	1.964 (2)
Co1–N2	1.947 (2)	Co1–N5	1.946 (2)
Co1–N3	1.964 (2)	Co1–N6	1.965 (2)
N2–Co1–N1	90.82 (9)	N5–Co1–N4	90.74 (9)
N2–Co1–N3	90.77 (9)	N5–Co1–N6	90.60 (9)
N1–Co1–N3	178.38 (9)	N4–Co1–N6	178.65 (9)
N2–Co1–N4	89.27 (9)	N5–Co1–N3	90.60 (9)
N2–Co1–N6	89.39 (9)	N5–Co1–N1	88.89 (9)
N2–Co1–N5	179.71 (10)	N3–Co1–N4	92.84 (9)
N1–Co1–N4	86.86 (9)	N3–Co1–N6	87.05 (9)
N1–Co1–N6	93.29 (9)		
N2–C10–C8–C9	35.6 (4)	N5–C33–C31–C32	36.1 (4)
N2–C14–C15–C20	34.9 (4)	N5–C37–C38–C43	35.1 (4)
2B			
Co2–N7	1.956 (2)	Co2–N10	1.961 (2)
Co2–N8	1.946 (2)	Co2–N11	1.946 (2)
Co2–N9	1.971 (2)	Co2–N12	1.961 (2)

Table 2. Cont.

N8–Co2–N7	89.87 (9)	N11–Co2–N10	90.10 (9)
N8–Co2–N9	90.01 (9)	N11–Co2–N12	90.00 (9)
N7–Co2–N9	179.85 (11)	N10–Co2–N12	179.50 (10)
N8–Co2–N10	89.79 (9)	N11–Co2–N9	89.99 (9)
N8–Co2–N12	90.10 (9)	N11–Co2–N7	90.14 (9)
N8–Co2–N11	179.89 (12)	N10–Co2–N9	93.03 (9)
N7–Co2–N10	87.05 (9)	N12–Co2–N9	87.46 (9)
N7–Co2–N12	92.46 (9)		
N8–C60–C58–C59	33.6 (4)	N11–C87–C88–C93	35.6 (4)
N8–C64–C65–C70	36.4 (4)	N11–C83–C81–C82	34.9 (4)

high-spin state for the coordination octahedron is much less distorted than in the low-spin state^{28,29}. The structural data obtained for **1** suggests a major contribution of low-spin species; however, contributions from high-spin species can not be ruled out solely on this data.

The X-ray crystal structure for the trication of $[\text{Co}(\text{mer-}\mathbf{bqp}\text{-}\kappa^3N,N',N'')_2][\text{Br}_3]_3$ is shown in (Fig. 2), with selected bond lengths and angles given in Table 2. Structure analysis of **2** reveals that two crystallographically independent (2A and 2B, Fig. 2) but chemically equivalent units compose the asymmetric unit. In contrast to complex **1**, the coordination environment proximate to the Co(III)-**bqp** ligand core remains near-equivalent. As a result, for 2A and 2B one set of complementary dihedral angles of approximately 36° and 35° represent the quinolines and central pyridine ring systems for each **bqp** ligand. Likewise, the average resultant bite angle for both 2A and 2B is 179°.

Quinoline $N_{Qn}Co^{III}$ and central pyridine ring system $N_{Py}Co^{III}$ bond lengths are 1.960 Å (average) and 1.946 Å, respectively, for both **2A** and **2B**. Comparatively, tetragonal compression is minimized relative to **1** allowing assignment as a low-spin d^6 complex of O_h symmetry *viz.* absence magnetic susceptibility for this redox state as discussed further below.

Of particular significance is how the geometry around the cobalt metal ions in **1** and **2** is closer to octahedral (O_h) geometry than their cobalt bis(terpyridine) analogs as a result of the larger bite angles of the **bqp** ligand (Appendix, Table S1). For $[Co(mer-tpy-\kappa^3N,N',N'')_2]^{2+}$, N–Co–N intraligand and bite angles are 85° and 157°, respectively. Those for $Co(mer-tpy-\kappa^3N,N',N'')_2]^{3+}$ are 85° and 157° and 89° and 164°, respectively. The Co– N_{Py} and Co– N_{Qn} bond lengths are notably shorter: 1.913 Å and 2.083 Å for $[Co(mer-tpy-\kappa^3N,N',N'')_2]^{2+}$ and 1.864 Å and 1.931 Å for $[Co(mer-tpy-\kappa^3N,N',N'')_2]^{3+}$. The terpyridine ligands occupy equivalent coordination environments around the Co(II) metal core, in contrast to that of **1**.

In comparison to other 3d metals, coordination of **bqp** to manganese generating the 5-coordinate $Mn(mer-bqp-\kappa^3N,N',N'')Cl_2$ has been reported³⁰. Similar to complexes **1** and **2**, the **bqp** ligand is coordinated in a tridentate fashion and is meridionally arranged about the manganese core. In addition, a twisted arrangement about the manganese core exists. However, a non-octahedral arrangement relative to the manganese center stands in contrast to that for complexes **1** and **2**. For the $Mn(mer-bqp-\kappa^3N,N',N'')Cl_2$, N–Mn–N intraligand and bite angles are 80° and 160°, respectively. The Mn– N_{Py} and Mn– N_{Qn} bond lengths are notably longer: 2.186 Å and 2.269 Å (average) for

Mn(*mer*-bqp- κ^3N,N',N'')Cl₂. As such, these measurements bear a closer resemblance to those for [Co(*mer*-tpy- κ^3N,N',N'')₂]ⁿ⁺ (*n* = 2, 3), than those for [Co(*mer*-bqp- κ^3N,N',N'')₂]ⁿ⁺ (*n* = 2, 3), complexes **1** and **2**.

DFT calculations were used to optimize the doublet and singlet ground state geometries for both complexes **1** and **2**, respectively. A complete listing of spin related transitions, Mulliken population analyses, and optimized structural data can be found in the Appendix. In general, DFT results describe experimental data well. The optimized

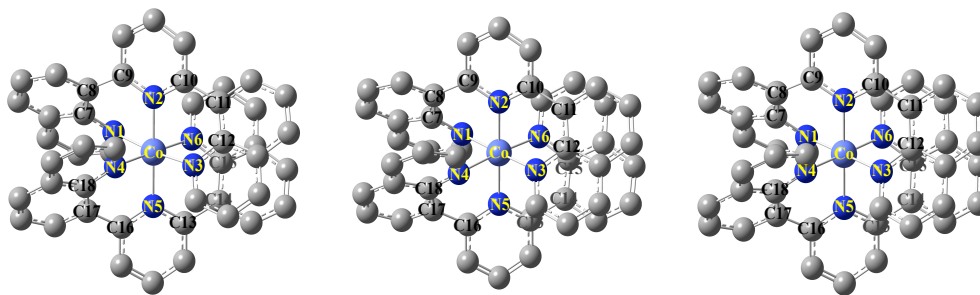


Figure 3. DFT (B3LYP/LANL2DZ) optimized structures of high-spin *mer,mer*-[Co(bqp- κ^3N,N',N'')₂]²⁺ (left, Mulliken spin density at Co: 2.659), low-spin [*mer,mer*-[Co(bqp- κ^3N,N',N'')₂]²⁺ (center, Mulliken spin density at Co: 0.938) and *mer,mer*-[Co(bqp- κ^3N,N',N'')₂]³⁺ (right) including a solvent model (CH₃CN).

structures for **1** and **2** show the twisted, near-octahedral arrangement relative to the cobalt core center (Fig. 3 and Appendix). For structure **1**, the energy for the low-spin state is lower than the high-spin state by 25.3 kJ mol⁻¹. Two complementary dihedral angles of approximately 42° (for both dihedral angles of one **bqp** ligand) and 37° (for both dihedral angles of the second **bqp** ligand) exist between the quinolines (Qn) and central pyridine (Py) ring systems. These angles differ somewhat relative to the characterized X-ray structure, but show the **bqp** ligands to be non-equivalent for the Co(II) low-spin complex.

The coordination environment proximate to the Co(III)-**bqp** ligand core remains near-equivalent. One dihedral angle of approximately 35° represents the quinolines and central pyridine ring systems for each **bqp** ligand. In contrast to **1**, calculated dihedral angles for **2** show excellent agreement relative to the characterized structure. For [Co(*mer*-**bqp**-κ³N,N',N'')₂][PF₆]₂ (**1**, low-spin), calculated N–Co–N intraligand and bite angles are 89° and 179° and 88° and 176°, respectively. And for [Co(*mer*-**bqp**-κ³N,N',N'')₂][Br₃]₃ (**2**, low-spin) are 89° and 177°, respectively. These N–Co–N intraligand and bite angles, on average, fall within hundredths of a degree (0.05°) compared to experimental. Calculated Co–N_{Py} and Co–N_{Qn} bond lengths are: 2.006 Å and 2.286 Å and 1.976 Å and 2.062 Å, respectively, for each **bqp** ligand for [Co(*mer*-**bqp**-κ³N,N',N'')₂][PF₆]₂ (**1**, low-spin), and 1.984 Å and 2.006 Å for [Co(*mer*-**bqp**-κ³N,N',N'')₂][Br₃]₃ (**2**, low-spin) indicative of its near-equivalent environment. The calculated bond lengths are marginally larger than experimental by 0.03 Å (average). However, it has to be noted that calculations at this level of theory predict slightly elongated bond lengths underestimating the ligand-induced strain and, as a result, tetragonal compression is underestimated²⁷.

2.5.2. Magnetic susceptibility

Magnetic susceptibility measurements were carried out at room temperature based on Evan's method³¹. Typically, the effective magnetic moment (μ_{eff}), assuming only the spin angular momentum, for bis(terpyridine) Cobalt(II) low-spin systems range between 2.0 and 2.7 BM (Bohr Magnetrons), while high-spin systems exhibit between 4.3 and 5.2

BM³². The d⁷ bis(8'-quinolinyl)pyridine Co(II) complex **1** produced an effective magnetic moment of 3.8 BM. Comparatively, the d⁷ bis(terpyridine) Co(II) complex, complex **3**, produced an effective magnetic moment of 3.1 BM^{32a}. The μ_{eff} for both complexes are consistent with a predominantly high-spin configuration, however, the μ_{eff} for **1** suggests a higher proportion of the high-spin configuration relative to **3** and is similar in magnitude to other bis(terpyridine) Co(II) high-spin systems^{32a}. This result combined with X-ray crystallography data allows us to assign a tetragonally compressed pseudo- D_{4h} geometry for **1** with the electronic configuration $b_{2g}^2 e_g^3 b_{1g}^1 a_{1g}^1$.¹

On the other hand, the d⁶ bis(8'-quinolinyl)pyridine Co(III) complex, complex **2**, produced no observable effective magnetic moment, consistent with a low-spin configuration. This was expected since bis(terpyridine) Cobalt(III), is known to exhibit a stable low-spin diamagnetic behavior at room temperature. This result, combined with X-ray crystallography data allows us to assign an octahedral geometry for **2** with the electronic configuration t_{2g}^6 .

2.5.3 Electronic spectra

Electronic data were recorded for these complexes in acetonitrile and the prominent peaks are recorded in Table 3. (Figure 4) shows the electronic spectrum for complexes **1** and **2** plotted as molar absorptivity *versus* wavelength. This allows a direct comparison of transition energies plus a measure of oscillator strengths. For both complexes absorption in the visible spectral region is low. Both complexes exhibit intense absorptions in the 200–380 nm region, which are consistent with π - π^* ligand centered transitions, as found with prior work for cobalt(III)-terpyridine complexes^{29,33}.

Absorptions between 400–550 nm are consistent with charge transfer transitions, as indicated by their low molar absorptivities and large full width half maxima (~21 590 and 20 500 cm^{-1} for **1** and **2**, respectively).

For the complexes investigated in this study, emission is not observed at room temperature or at 77 K. DFT and TD-DFT calculations have been widely used in the

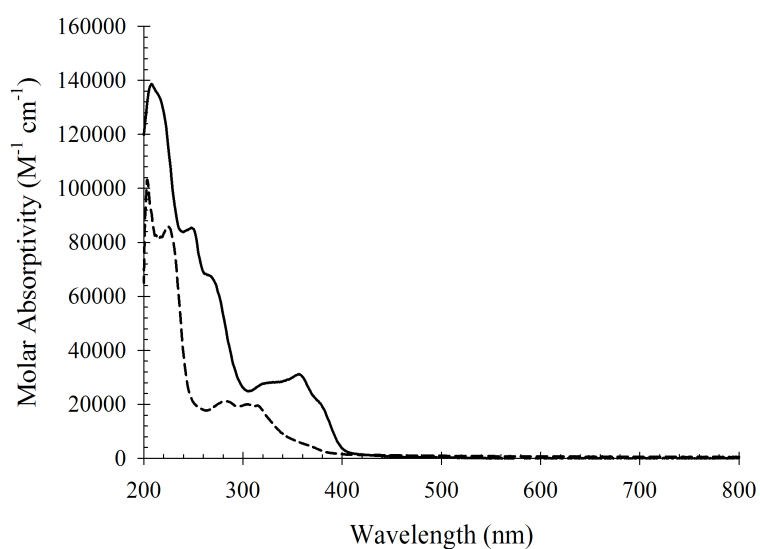


Figure 4. Absorption spectra for *mer,mer*-[Co(bqp- κ^3 N,N',N'')₂]²⁺ (**1**; black, short dash) and *mer,mer*-[Co(bqp- κ^3 N,N',N'')₂]³⁺ (**2**; black, solid line) in acetonitrile at room temperature.

study of metal polypyridine complexes because of their utility and relative accuracy in providing insight into the structural and electronic properties of such systems³⁴. DFT and TDDFT have been performed on both complexes **1** and **2** at the B3LYP/6-31 g*(C,H,N) and LANL2DZ(Co) level of theory with an acetonitrile polarizable continuum solvent model. A complete listing of spin related transitions, Mulliken population analysis, and

optimized structural data can be found in the Appendix. As an example, (Figure 5) illustrates the predominant molecular orbitals involved in the observed electronic transitions for $[\text{Co}(\text{mer-bqp-}\kappa^3\text{N},\text{N}',\text{N}'')_2][\text{Br}_3]_3$ (**2**).

Table 3. Electronic absorption maxima.^a

Complex	λ_{max} (nm) ($\times 10^3$ ($\text{M}^{-1} \text{cm}^{-1}$))
$[\text{Co}(\text{mer-bqp-}\kappa^3\text{N},\text{N}',\text{N}'')_2][\text{PF}_6]_2$	203 (102.4), 225 (85.8), 282 (21.2), 306 (19.9), 315 (19.5), 364 (5.1; br.), 460 (1.1; br.)
$[\text{Co}(\text{mer-bqp-}\kappa^3\text{N},\text{N}',\text{N}'')_2][\text{Br}_3]_3$	204 (102.6), 206 (95.2, sh.), 225 (86.2), 282 (21.2), 305 (20.0), 314 (19.6), 360 (5.5, sh.), 461 (1.1, br.)

^a In acetonitrile (CH_3CN) solvent; sh = shoulder, br = broad.

The molecular orbitals shown in Figure 5 provide a convenient visual descriptor for the calculated electronic transitions of $[\text{Co}(\text{mer-bqp-}\kappa^3\text{N},\text{N}',\text{N}'')_2][\text{Br}_3]_3$ (**2**) which show a composite of many molecular orbitals with varying contributions. In general, electronic transitions in the region 400–550 nm are best represented as ligand-to-metal and metal-to-ligand charge transfers. By way of illustration, the transition calculated at 444.1 nm shows a significant (HOMO–1)-to-LUMO contribution with a percentage contribution to the electronic transition at 49%. From the (HOMO–1), it can be seen that the HOMO–1 character of this transition is predominantly **bqp** based. The LUMO is composed of 56% cobalt and 44% **bqp**. Electronic transitions in the region 200–400 nm are best characterized as ligand-to-ligand. The transition calculated at 298.8 nm shows a significant (HOMO–4)-to-(LUMO+6) contribution with a percentage contribution to the excited state at 40%. Both the (HOMO–4) and (LUMO+6) are ligand based. The

oscillator strengths are indicative of intraligand transitions. These results are consistent

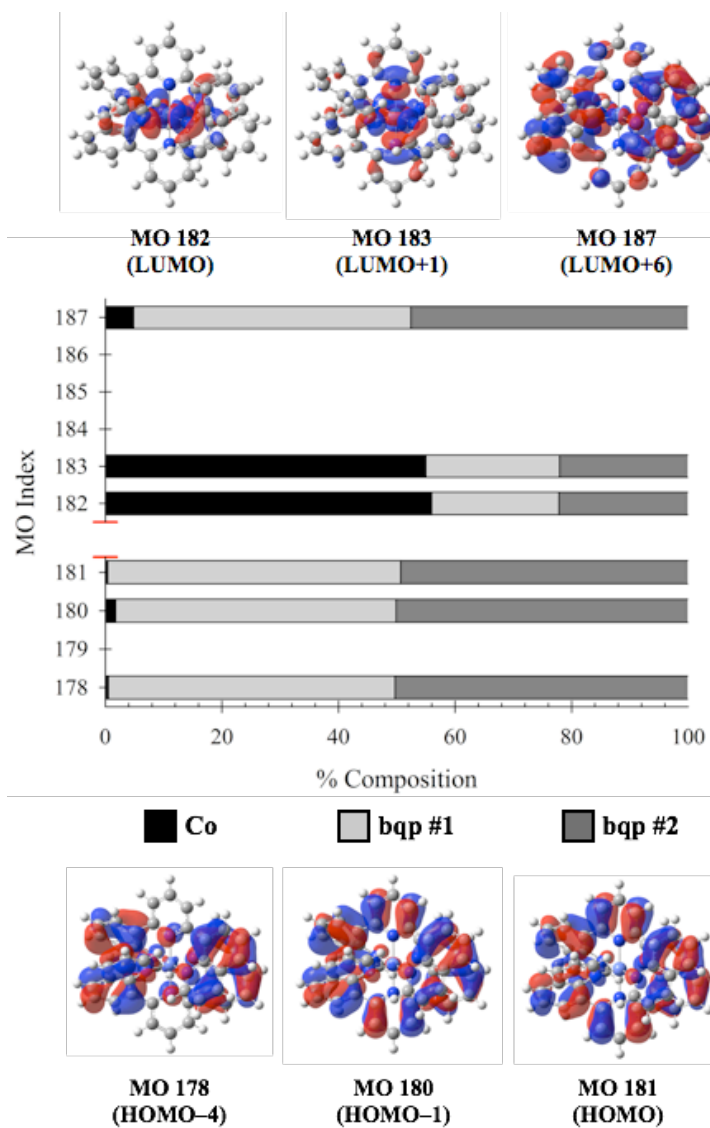


Figure 5. Comparison of molecular orbitals for $mer,mer-[Co(bqp-\kappa^3N,N',N'')_2]^{3+}$ (2) derived from DFT calculation at the B3LYP/LAN2DZ level. HOMO is orbital #181. The horizontal bars correspond to the orbitals as numerated on the left axis. The color codes define the sum of the squares of the molecular orbital coefficients of the total atomic contributions from the cobalt and both bqp-ligands as noted. In the case of the metal, the cobalt contributions includes, in addition to d contributions, very small s and p contributions so that the total sums to unity.

with the assignments of the experimental absorption spectrum described earlier. The

electronic transitions by TD-DFT using the B3LYP functional with inclusion of solvent CH₃CN described by the conductor-like polarization continuum model (CPCM) correspond very well with the experimental data. As an example, the experimental UV–vis and corresponding simulated UV–vis absorption spectrum (both in acetonitrile solvent) for [Co(*mer*-**bpq**-κ³N,N',N'')₂][Br₃]₃ (**2**), are shown in (Figure 5). The simulation

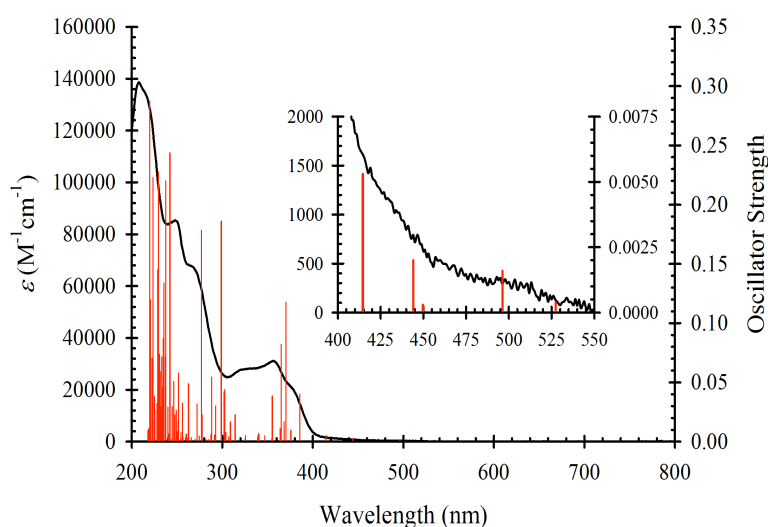


Figure 6. Simulated absorption spectrum for *mer,mer*-[Co(*bpq*-κ³N,N',N'')₂]³⁺ (**2**), red bars) in acetonitrile and the experimental absorption spectrum measured in acetonitrile (solid line). Top right inset shows the region between 350–800 nm.

was performed using SWizard software³⁰. All calculated transitions are included. Bar heights are proportional to calculated oscillator strengths. A very similar spectrum is obtained (see Figure 6).

2.5.4 Electrochemistry

Cyclic voltammetry was recorded for both **1** and **2** dissolved in acetonitrile-TBAPF₆ media. Representative voltammograms for [Co(*mer*-**bqp**-κ³N,N',N'')₂][PF₆]₂ (**1**) and [Co(*mer*-bqp-κ³N,N',N'')₂][Br₃]₃ (**2**) are shown in Figure 7. Complex **1** undergoes two one-electron reversible processes with redox potentials of +0.43 and -0.85 V (vs. SCE). The single reversible oxidation wave observed at +0.43 V (vs. SCE) corresponds to a

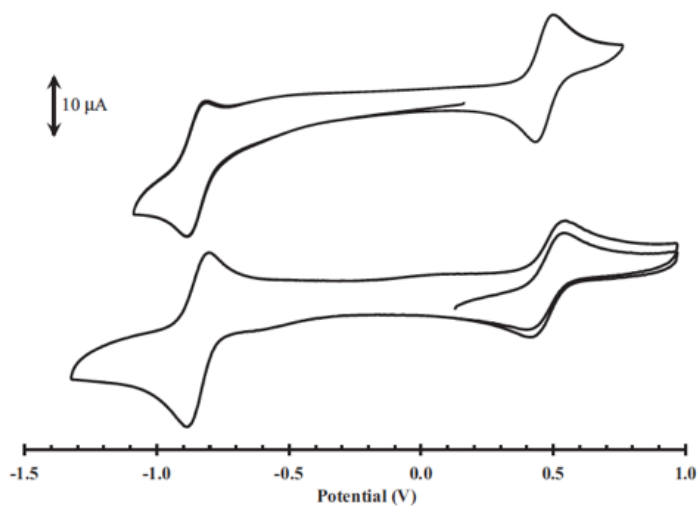


Figure 7. Cyclic voltammograms for *mer,mer*-[Co(bqp-κ³N,N',N'')₂]³⁺ (**2**, top) and *mer,mer*-[Co(bqp-κ³N,N',N'')₂]²⁺ (**1**, bottom). Scan rate: 0.10 V s⁻¹. Direction of scan: oxidative-to-reductive. Potential (V vs. SCE).

Co(III/II) based redox couple and which is higher than the corresponding [Co(*mer*-tpy-κ³N,N',N'')₂]²⁺ complex ($E_{1/2} = +0.28$ V vs. SCE)^{36,33}. Considering the similar pK_a values for quinoline and pyridine, 4.94 and 5.20, respectively³⁷ this data implies more efficient π back-bonding in **1** relative to [Co(*mer*-tpy-κ³N,N',N'')₂]²⁺. In contrast, the Ru(III/II) couple of the [Ru(*mer*-**bqp**-κ³N,N',N'')₂]²⁺ complex ($E_{1/2} = +0.71$ V versus SCE) is lower than in [Ru(*mer*-tpy-κ³N,N',N'')₂]²⁺ ($E_{1/2} = +0.92$ V versus SCE) indicating less efficient

π back-bonding^{14b}. The reversible reduction wave observed at -0.85 V (vs. SCE) is assigned as a ligand-based (**bqp**^{0/-}) reduction and occurs at a more negative potential than the corresponding $[\text{Co}(\text{mer-tpy-}\kappa^3\text{N,N',N''})_2]^{2+}$ complex at $E_{1/2} = -0.77$ V versus SCE³².

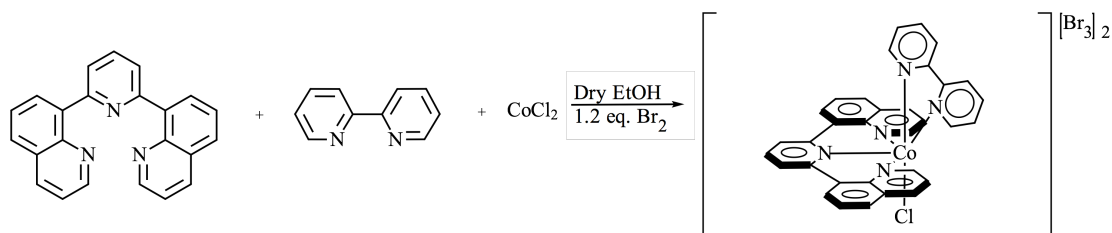
For both complexes **1** and **2**, an additional irreversible reduction is observed at potentials -1.56 and -1.58 V (vs. SCE), respectively. These are defined as a ligand localized reduction in accordance with previous literature³⁸ and³⁹. For each of these complexes, sweeping through this second reduction lead to reductive degradation.

CHAPTER 3

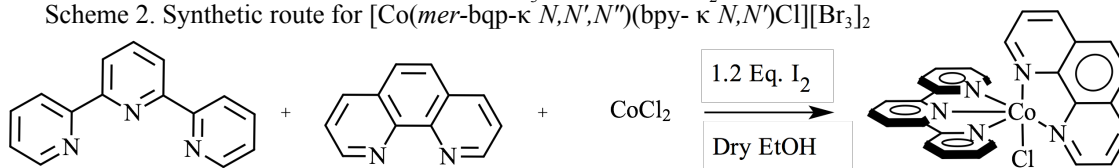
3. HETEROLEPTIC COMPLEXES

3.1. General remarks

Cobalt(II) chloride, $\text{Co}(\text{Cl})_2 \cdot 6\text{H}_2\text{O}$, ammonium hexafluorophosphate (NH_4PF_6) and iodine (I_2) were purchased from Aldrich and used without further purification. The 2,6-bis(8'-quinolinyl)pyridine (**bqp**) ligand was prepared in accordance to a previous



Scheme 2. Synthetic route for $[\text{Co}(\text{mer-bqp-}\kappa^3\text{N,N',N''})(\text{bpy-}\kappa^2\text{N,N'})\text{Cl}][\text{Br}_3]_2$



Scheme 3. Synthetic route for $[\text{Co}(\text{mer-tpy-}\kappa^3\text{N,N',N''})(\text{phen-}\kappa^2\text{N,N'})\text{Cl}][\text{PF}_6]_2$

literature report¹².

All solvents for synthesis were of reagent grade and used as received, unless otherwise specified, see Section 2.1.

3.2. Physical measurements

See Section 2.2.

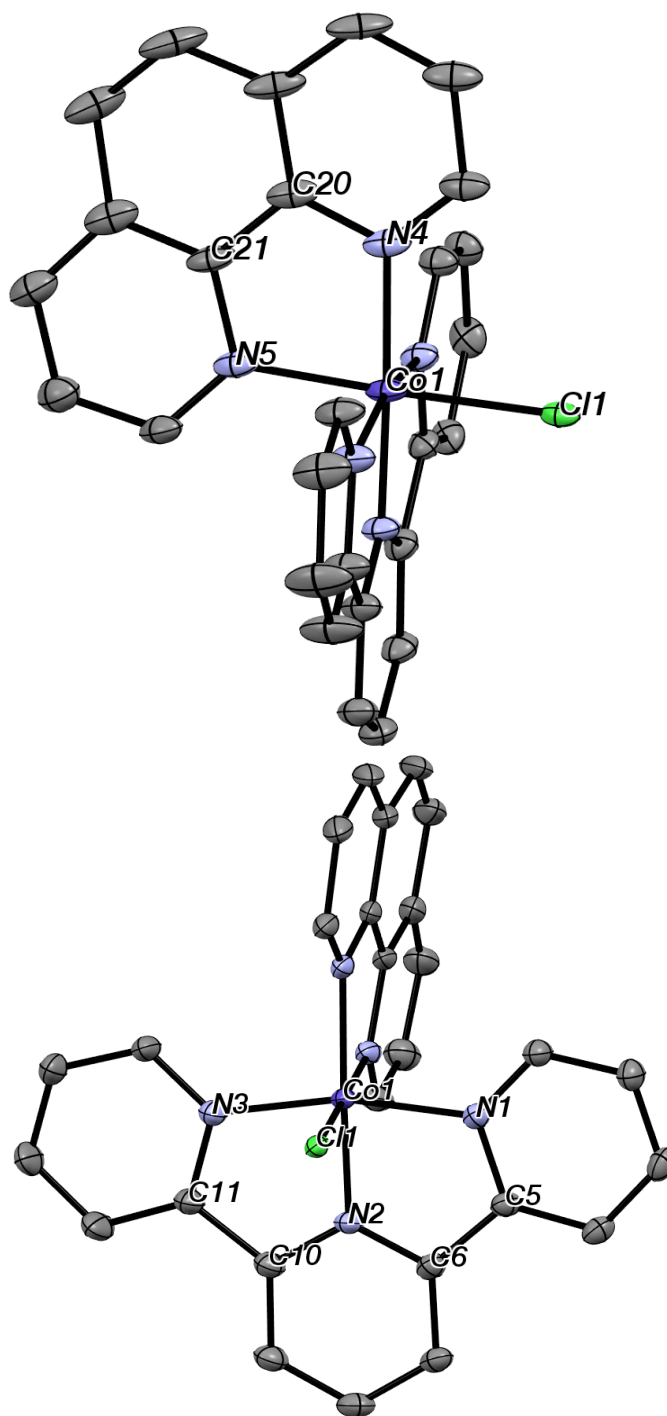


Figure 8: Solid-state structure of $[\text{Co}(\text{mer-tpy-}\kappa^3\text{N,N',N''})(\text{phen-}\kappa^2\text{N,N',N''})\text{Cl}][\text{PF}_6]_2$ with the perspective of the **tpy** plane (top) and the **phen** plane (bottom) for emphasis of the near octahedral geometry (hydrogens are omitted for clarity).

3.3. Synthesis of Heteroleptic Complexes

3.3.1 Synthesis of $\text{Co}(\text{mer-bqp-}\kappa^3\text{N,N',N''})(\text{bpy-}\kappa^2\text{N,N'})\text{Cl}[\text{PF}_6]_2$ (5)

The heteroleptic complex (5) was obtained by stirring a 1:1:1 mixture of dry CoCl_2 (1.6×10^{-4} mol) the desired **bqp** (1.6×10^{-4} mol) ligand, and the desired **bpy** (1.6×10^{-4} mol) ligand in deoxygenated, anhydrous ethanol for 6h (Scheme 2). The crude product was precipitated with Br_2 (1.9×10^{-4} mol) and collected via vacuum filtration. This was followed by purification using a neutral alumina column using hexane followed by dichloromethane, then methanol (impure by-product eluted here), and finally acetonitrile to elute the desired heteroleptic product.

The use of Br_2 as an oxidant in the latter reaction was done because I_2 simply wasn't a strong enough oxidant. The major products obtained by using I_2 were the $\text{Co}(\text{bqp})_2^{2+}$ and $\text{Co}(\text{phen})_3^{2+}$ complexes. By using Br_2 a high yield of byproducts was avoided and the heteroleptic complexes were synthesized successfully. ^1H NMR ($\text{CD}_3\text{CN-}d_3$): δ 8.88 (dd, $J = 6.43$ Hz, 1H), 8.76 (dd, $J = 5.06$ Hz, 1H), 8.64 (dd, $J = 4.41$ Hz, 4H), 8.52 (m, 2H), 8.47 (t, $J = 7.92$ Hz, 2H), 8.36 (dd, $J = 4.78$ Hz, 2H), 8.09 (d, $J = 7.91$ Hz, 2H), 8.06 (dd, $J = 3.45$, 2 Hz), 8.03 (dd, $J = 4.34$, 2 Hz), 7.99 (m, 1 Hz), 7.94 (dd, $J = 4.75$, 2 Hz), 7.84 (dd, $J = 6.43$, 1 Hz), 7.70 (dd, $J = 7.85$, 3 Hz), 7.43 (dd, $J = 6.79$, 3 Hz). ^{13}C NMR ($\text{CD}_3\text{CN-}d_6$): δ 163.3, 155.8, 150.8, 145.1, 144.6, 143.8, 134.5, 134.0, 130.9, 129.5, 129.2, 128.5, 128.1, 125.3, 124.9, 123.5.

3.3.2 Synthesis of $\text{Co}(\text{mer-tpy-}\kappa^3\text{N,N',N''})(\text{phen-}\kappa^2\text{N,N'})\text{Cl}[\text{PF}_6]_2$ (3) and $\text{Co}(\text{mer-tpy-}\kappa^3\text{N,N',N''})(\text{bpy-}\kappa^2\text{N,N'})\text{Cl}[\text{PF}_6]_2$ (4)

The heteroleptic complex (**3**) was obtained by stirring a 1:1:1 mixture of anhydrous CoCl_2 (8.0×10^{-4} mol) the desired **tpy** ligand (8.0×10^{-4} mol), and the desired **phen** ligand (8.0×10^{-4} mol) in deoxygenated, anhydrous ethanol for 4h (Scheme 3). The crude product was precipitated with I_2 (1.02×10^{-3} mol) and collected via vacuum filtration which was followed by further purification using a neutral alumina column using hexane followed by dichloromethane, then methanol (impure by-product eluted here), and finally acetonitrile to elute the desired heteroleptic product. The acetonitrile fraction was then stirred with excess ammonium hexafluorophosphate to exchange the counterion. This was dried under reduced pressure and produced a 0.298g (0.374 mmol) 56% yield. ^1H NMR ($\text{CD}_3\text{CN}-d_3$): δ 10.23 (dd, $J = 5.47$ Hz, 1H), 9.32 (dd, $J = 8.33$ Hz, 1H), 8.91 (dd, $J = 8.98$ Hz, 4H), 8.84 (m, 2H), 8.63 (dd, $J = 8.69$ Hz, 2H), 8.69 (dd, $J = 8.17$ Hz, 2H), 8.63 (dd, $J = 8.31$ Hz, 2H), 8.56 (dd, $J = 7.94$ Hz, 2H), 8.52 (d, $J = 8.86$, 2H), 8.31 (d, $J = 8.93$ Hz, 1H), 8.20 (td, 2H), 7.64 (dd, $J = 8.18$ Hz, 1H), 7.44 (dd, $J = 5.49$ Hz, 3H), 7.34 (ddd, $J = 7.43$, 2H), 7.20 (m, 3H). ^{13}C NMR ($\text{CD}_3\text{CN}-d_6$): δ 157.4, 157.1, 156.8, 156.2, 153.7, 153.2, 152.1, 148.4, 146.8, 146.6, 144.9, 144.0, 142.9, 142.8, 141.7, 133.2, 132.6, 131.8, 130.7, 129.7, 129.4, 129.3, 128.7, 128.6, 128.1, 127.3, 127.1.

The heteroleptic complex (**4**) was obtained by stirring a 1:1:1 mixture of anhydrous CoCl_2 (2.0×10^{-3} mol) the desired **tpy** ligand (2.0×10^{-3} mol), and the desired **bpy** ligand (2.0×10^{-3} mol) in deoxygenated, anhydrous ethanol for 4h (Scheme 3). The crude product was precipitated with I_2 (2.4×10^{-3} mol) and collected via vacuum filtration which was followed by further purification using a neutral alumina column using hexane followed by dichloromethane, then methanol (impure by-product eluted here), and finally

acetonitrile to elute the desired heteroleptic product. The acetonitrile fraction was then stirred with excess ammonium hexafluorophosphate to exchange the counterion. This was dried under reduced pressure and produced a 0.798g (1.03 mmol) 42% yield. Both ^1H and ^{13}C NMR matched previous data reported by Jackson et al³⁹.

3.4 Characterization of $[\text{Co}(\text{mer-tpy-}\kappa^3\text{N},\text{N}',\text{N}'')(\text{phen-}\kappa^2\text{N},\text{N}')\text{Cl}][\text{PF}_6]_2$

3.4.1. Ligand Synthesis

See section 2.5.1 for synthesis.

3.4.2. X-Ray Crystallography

Crystals of **3** and **4** were grown by slow evaporation in acetonitrile. Structural analysis for **4** reveals a perpendicular, near-octahedral arrangement relative to the cobalt center. The 2,2':6',2''-terpyridine (**tpy**), and 1,10-phenanthroline (**phen**) are coordinated tridentate and bidentate, respectively, and are meridionally arranged about the cobalt core with resultant **tpy** and **phen** ligands coordination planes lying perpendicular to each other. No evidence for facial isomers was

Table 4: Selected bond lengths and angles for $[\text{Co}(\text{mer-tpy-}\kappa^2\text{N},\text{N}',\text{N}'')(\text{phen-}\kappa^2\text{N},\text{N}',\text{N}'')]\text{Cl}_2$

Bond	Length (Å)	Bond	Length (Å)
Co1–N1	1.946 (2)	Co1–N4	1.950 (2)
Co1–N2	1.855 (2)	Co1–N5	1.953 (3)
Co1–N3	1.933 (2)	Co1–Cl1	2.2439 (9)
Bonds	Angle (°)	Bonds	Angle (°)
N2–Co1–N1	82.9 (1)	N5–Co1–N4	84.1 (1)
N2–Co1–N3	83.1 (1)	N5–Co1–Cl1	177.89 (8)
N1–Co1–N3	166.0 (1)	N4–Co1–Cl1	93.87 (8)
N2–Co1–N4	177.2 (1)	N5–Co1–N3	91.01 (1)
N2–Co1–Cl1	88.43 (8)	N5–Co1–N1	90.1 (1)

Table 4. Cont.

N2–Co1–N5	93.5 (1)	N3–Co1–N4	98.5 (1)
N1–Co1–N4	95.5 (1)	N3–Co1–Cl1	89.95(8)
N1–Co1–Cl1	89.44 (7)		

found. This stands in contrast to previous reports where coordination of **tpy/bpy** to a cobalt(III) core produced both facial and meridional isomers³⁹. It stands to reason, the cobalt(III) core allows the **tpy** ligand to optimally orientate upon coordination resulting in the meridional arrangement, which leaves one of the octahedral coordination sites vacant and can possibly be utilized for catalytic reactions.

Table 5: Selected bond lengths and angles for [Co(*mer*-tpy- κ^2N,N',N'')(bpy- κ^2N,N',N'')]²⁺

Bond	Length (Å)	Bond	Length (Å)
Co1–N1	1.937 (4)	Co1–N4	1.946 (4)
Co1–N2	1.850 (4)	Co1–N5	1.934 (5)
Co1–N3	1.958 (4)	Co1–Cl1	2.240 (2)
Bonds	Angle (°)	Bonds	Angle (°)
N2–Co1–N1	82.8 (2)	N5–Co1–N4	82.8 (2)
N2–Co1–N3	82.6 (2)	N5–Co1–Cl1	177.3 (1)
N1–Co1–N3	165.3 (2)	N4–Co1–Cl1	94.5 (1)
N2–Co1–N4	175.8 (2)	N5–Co1–N3	88.7 (2)
N2–Co1–Cl1	89.3 (1)	N5–Co1–N1	92.6 (2)
N2–Co1–N5	93.4 (2)	N3–Co1–N4	95.6 (2)
N1–Co1–N4	99.0 (2)	N3–Co1–Cl1	91.6 (1)
N1–Co1–Cl1	87.8 (1)		

The X-Ray crystal structure for the dication of **3** is show in Figure 8, with selected bond angles and lengths given in Table 3. The **tpy** ligand occupies a planar meridional

chelation around the Co(III) core, which leaves the chlorido ligand pointing linearly away from the cobalt(III) core to reduce steric hindrance. The bite angles for the **tpy** and **phen** ligands are 166.0° and 84.1° respectively. Similarly to $[\text{Co}(\text{mer-tpy-}\kappa^3\text{N},\text{N}',\text{N}'')_3]^{2+}$ ⁴⁰ the **phen** complexes show a small increase in Co-N bond lengths, being on average 0.0115 Å larger for the **phen** ligand than the **bpy** ligand (Table 4).

3.4.3. NMR Spectroscopy

Both $[\text{Co}(\text{mer-tpy-}\kappa^2\text{N},\text{N}',\text{N}'')(\text{phen-}\kappa^2\text{N},\text{N}',\text{N}'')\text{Cl}][\text{PF}_6]_2$ (**3**) and $[\text{Co}(\text{mer-tpy-}\kappa^2\text{N},\text{N}',\text{N}'')(\text{bpy-}\kappa^2\text{N},\text{N}',\text{N}'')\text{Cl}][\text{PF}_6]_2$ (**4**) complexes can exist in three isomeric forms *mer*,

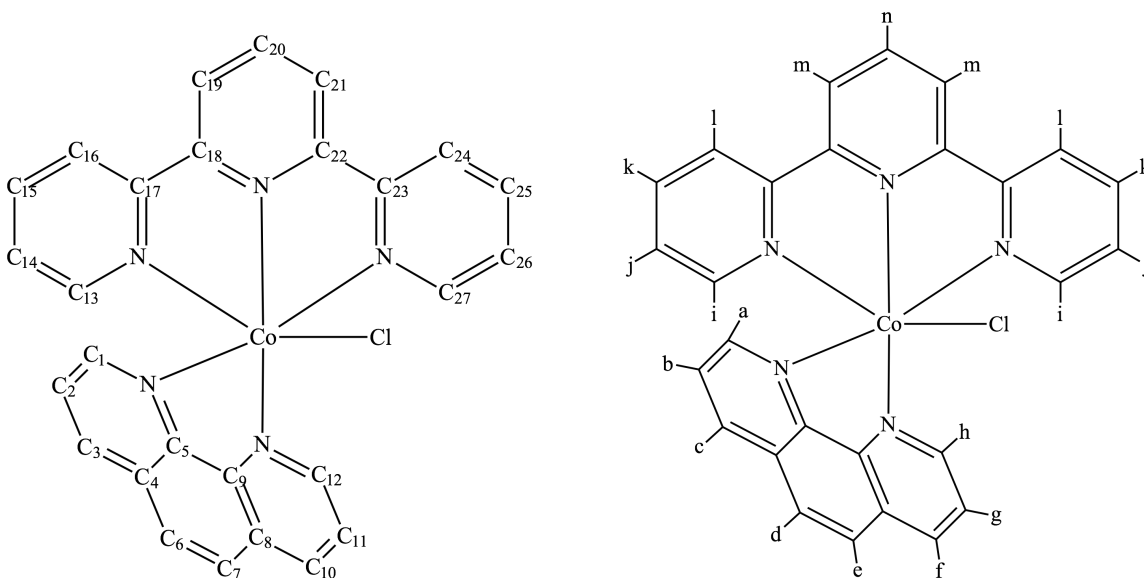


Figure 9: $[\text{Co}(\text{mer-tpy-}\kappa^3\text{N},\text{N}',\text{N}'')(\text{phen-}\kappa^2\text{N},\text{N}',\text{N}'')\text{Cl}][\text{PF}_6]_2$

sym-fac, or *unsym-fac*. X-ray analysis shows our structure to be the *mer* isomer. NMR data for **4** has been assigned³⁹. As for complex **3** a plane of symmetry exists, thus for the 27 carbon atoms in the molecule, the number of peaks expected in the 1D ¹³C NMR spectrum should be 21(5 x 2 (C-H)) and (9 x 1 (C-H)), and (8 x 1 (C)). The ¹³C NMR shows that there are 21 resonances, five of these peaks are double the height of the others.

The missing peaks are thought to be the quaternary carbons found in this complex. This data is consistent with previous similar complexes indicating that it is the *mer* isomer.

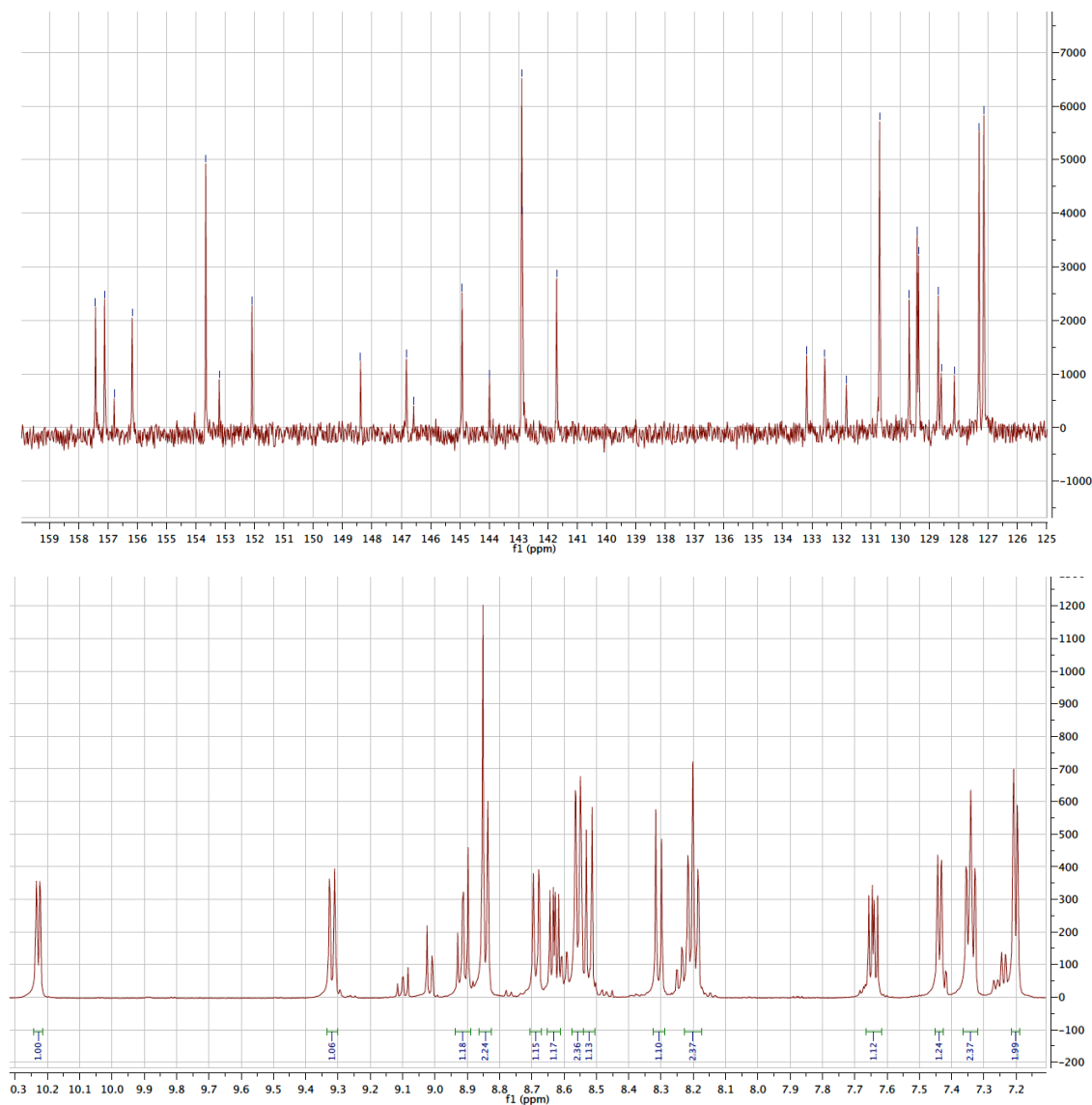


Figure 10: Spectra of $[\text{Co}(\text{mer-tpy-}\kappa^3\text{N,N',N''})(\text{phen-}\kappa^2\text{N,N}')\text{Cl}]^{2+}$. Top ^{13}C NMR Spectrum. Bottom ^1H NMR Spectrum.

This *mer* symmetry is also supported by the ^1H NMR spectrum. Fourteen C-H resonances are expected and observed; five of intensity of two and nine of intensity one, with the

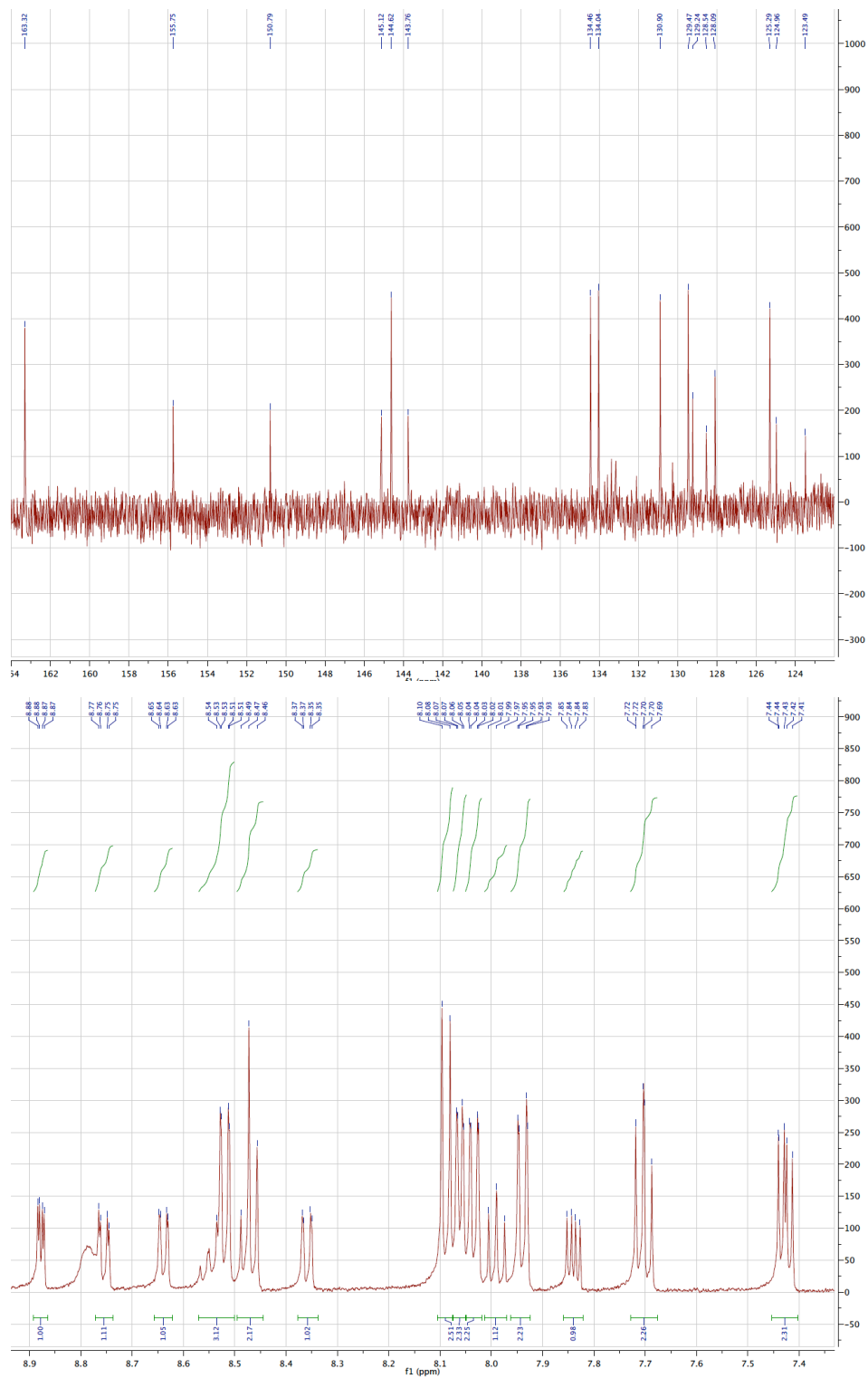


Figure 12: Spectra of $[\text{Co}(\text{mer-bqp-}\kappa^3\text{N,N,N}'')(\text{bpy-}\kappa^2\text{N,N}')\text{Cl}][\text{Br}_3]_2$. Top ^{13}C NMR Spectrum. Bottom ^1H NMR Spectrum.

outer aromatic signals appearing as doublets and the inner as triplets. The four groups of **tpy** and **phen** are defined by the ^1H NMR spectra (Figure 9/10). The resonances at 7.20, 7.34, 7.44, and 7.64 ppm represent a, b, c, and d; 8.52, 8.56, 8.63, and 8.69 ppm represent h, g, f, and e. The resonances of 8.20, 8.31, 8.84, 8.91, 9.32, and 10.23 ppm have been identified and are represented as such n, m, k, l, j, and i respectively. The i and j hydrogen peaks are further downfield due to the ligand bite angle which provides a close proximity to the chlorine ligand off of the cobalt, this data is similar and supported by previous $\text{Co}(\text{mer-tpy-}\kappa^3\text{N,N',N''})(\text{bpy-}\kappa^2\text{N,N'})\text{Cl}][\text{PF}_6]_2$ research³⁹. The carbon peaks for this

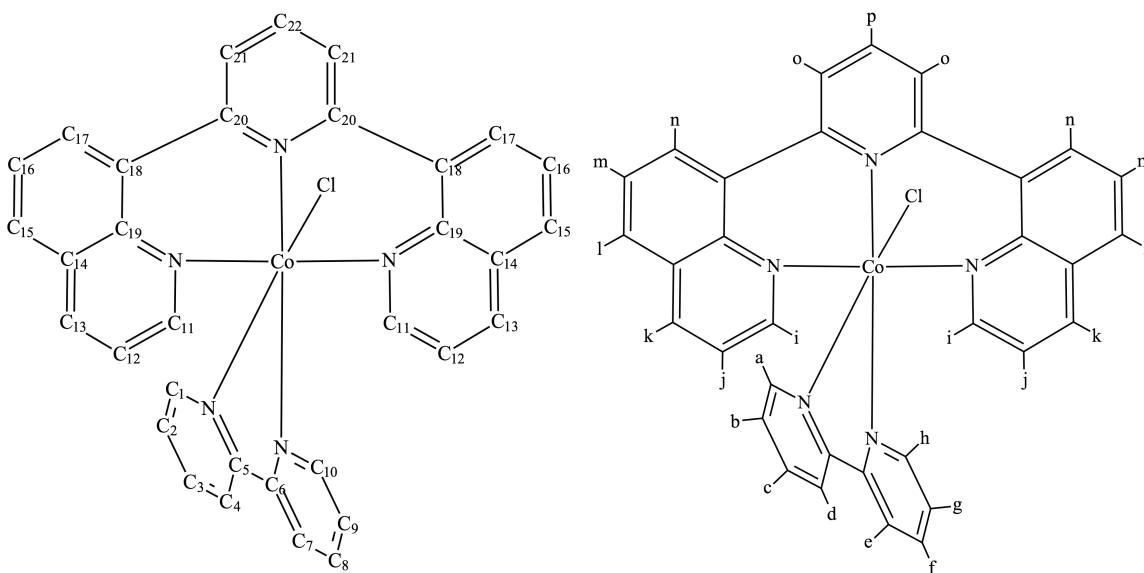


Figure 11: Marked $[\text{Co}(\text{mer-bqp-}\kappa^3\text{N,N',N''})(\text{bpy-}\kappa^2\text{N,N'})\text{Cl}][\text{Br}_3]_2$

complex are again easily identified. The resonances at 132.56, 133.18, 146.82, and 148.39 ppm represent C_{17} , C_{23} , C_{18} , and C_{22} ; the resonances at 128.14, 128.59, 131.82, 143.99, 146.57, 153.20, and 156.78 ppm represent C_4 , C_6 , C_7 , C_8 , C_5 , C_{20} , and C_9 ; the resonances at 128.69, 129.36, 129.42, 129.69, 141.70, 144.93, 152.09, 156.17, 157.11, and 157.42 ppm correspond to C_{15} , C_{19} , C_{21} , C_{25} , C_{16} , C_{24} , C_3 , C_{10} , C_{11} , and C_2 ; the

resonances at 127.14, 127.30, 130.70, 142.87, 142.89, and 153.66 ppm represent C₁, C₁₄, C₂₆, C₁₃, C₂₇, and C₁₂.

The [Co(*mer*-**bqp**- κ^3N,N',N'')(**bpy**- κ^2N,N')Cl][Br₃]₂ (**5**) complex can exist in three isomeric forms *mer*, *sym-fac*, or *unsym-fac*. Previously synthesized complexes have been shown to be the *mer* isomer through X-ray analysis, as such our structure is also thought to be the *mer* isomer. Unfortunately this complex starts to degrade in solvent almost immediately, therefore the spectra and figure shown are for an immediately purified sample. A plane of symmetry exists, thus for the 33 carbon atoms in the molecule, the number of peaks expected in the 1D ¹³C NMR spectrum should be 23(7 x 2 (C-H)) and (9 x 1 (C-H)). The ¹³C NMR shows that there are 16 resonances, seven of these peaks are double the height of the others. The missing peaks are the quaternary carbons found in this complex. This data is consistent with previous similar complexes indicating that it is the *mer* isomer. This *mer* symmetry is also supported by the ¹H NMR spectrum. Fourteen C-H resonances are expected and observed; six of intensity of two and six of intensity one, and two with an intensity of three, with the outer aromatic signals appearing as doublets and the inner as triplets. The four groups of **bqp** and **bpy** are defined by the ¹H NMR spectra (Figure 11/12) . The resonances at 7.84, 7.99, 8.36, 8.64, 8.75, and 8.87 ppm represent f, g, a, d, e, and h. The resonances of 7.43, 7.70, 7.95, 8.04, 8.05, and 8.48 ppm have been identified and are represented as such l, k, n, o, i, and b/c overlap respectively. The carbon peaks for this complex are again easily identified. The resonances at 125.29, 129.47, 130.90, 134.04, 134.46, 144.62, and 163.32 ppm represent C₂₁, C₁₇, C₁₆, and C₁₅, C₁₃, C₁₂, and C₁₁; the resonances at 123.49, 124.96, 128.09,

128.54, 129.24, 143.76, 145.12, 150.79, and 155.75 ppm represent C₁, C₂, C₂₂, C₃, C₄, C₇, C₈, C₉, and C₁₀.

3.4.4. Electrochemistry

Cyclic voltammetry was recorded for complexes **3**, **4**, and **5** which were dissolved in an acetonitrile-TBAPF₆ media. Representative voltammograms are shown for **3** and **4**, and **5** in Figure 13 and Figure 14, respectively. Figure 13 shows the measurements of four

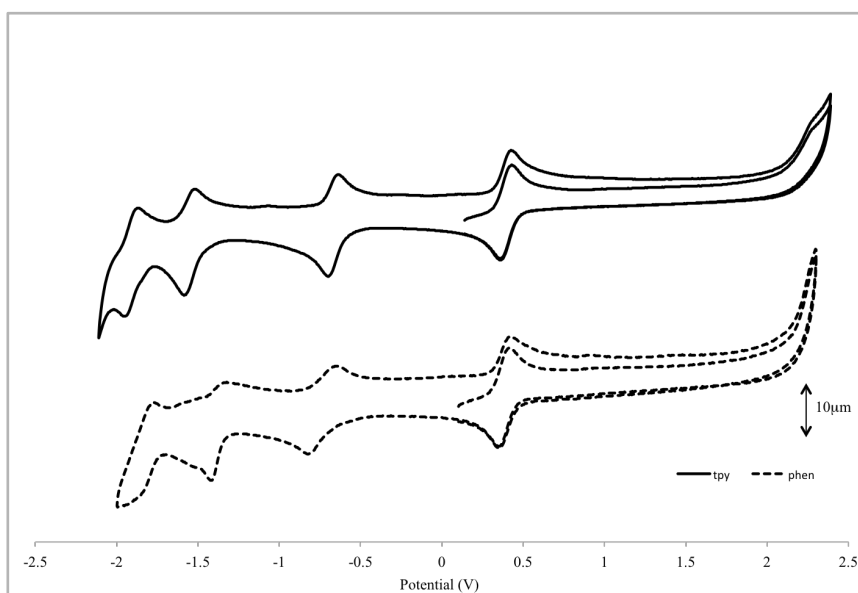


Figure 13: Selected voltammograms for [Co(*mer*-**tpy**- κ^3N,N',N'')(**bpy**- κ^2N,N')Cl][PF₆]₂, top, and [Co(*mer*-**tpy**- κ^3N,N',N'')(**phen**- κ^2N,N')Cl][PF₆]₂, bottom, in acetonitrile-TBAPF₆ media.

one-electron reversible processes for complex **3** with the E_{1/2} (ΔE_p) redox potentials at – 1.89(0.02) V, -1.38(0.04) V, and -0.74(0.16) V, and +0.39(0.04) V (vs. SCE). These redox processes are assigned as ligand-based (**phen**^{0/-}), Co^{I/II}, Co^{II/III}, and Co^{III/IV} couples, respectively^{41,42}. The potentials for complexes **3** and **4** are similar, as expected due to the structural (and electronic) similarities. For complex **4**, exchanging the **phen** for **bpy** results in a slight shift in the reduction potentials. These E_{1/2} (ΔE_p) reduction potentials

are observed at $-1.91(0.04)$ V, $-1.55(0.03)$ V, and $-0.67(0.03)$ V (*vs.* SCE) and are assigned as ligand-based ($\mathbf{tpy}^{0/-}$), $\text{Co}^{\text{I/II}}$, and $\text{Co}^{\text{II/III}}$ respectively. The oxidation peak at $+0.39$ V, which is the same potential as that found for complex **3**, and is assigned to the $\text{Co}^{\text{III/IV}}$ couple. As shown in Figure 13, complex **3** lacks the reversibility demonstrated with complex **4**. The larger ΔE_p values of the reductive peaks are indicative of quasi-irreversible reactions. This larger ΔE_p value also corresponds to a slower electron transfer

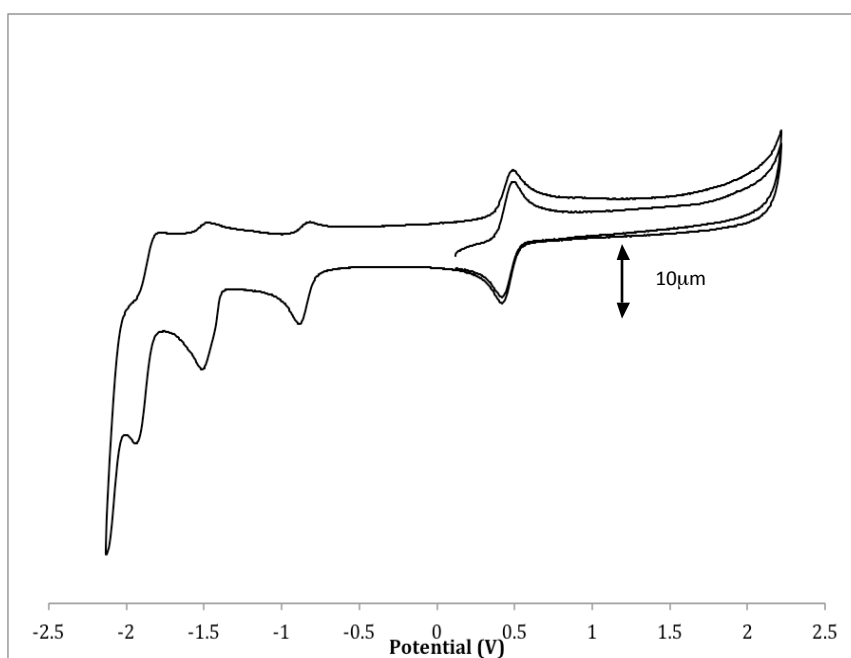


Figure 14: Selected voltammogram for $[\text{Co}(\text{mer-}\mathbf{bqp}\text{-}\kappa^3\text{N},\text{N}',\text{N}'')(\mathbf{bpy}\text{-}\kappa^2\text{N},\text{N}')\text{Cl}][\text{Br}_3]_2$ in acetonitrile-TBAPF₆ media.

caused by the large structural change. This implies there is a slight decomposition resulting from the redox reaction not going to completion.

Nagata *et al.* did similar work with $[\text{Co}(\text{mer-}\mathbf{tpy}\text{-}\kappa^3\text{N},\text{N}',\text{N}'')(\mathbf{bpy}\text{-}\kappa^2\text{N},\text{N}')\text{Cl}][\text{PF}_6]_2$, although in their case the **tpy** and **bpy** ligand were linked together with poly-methylene chains¹³ with $E_{1/2}$ (ΔE_p) redox potentials at $-1.72(0.07)$ V, $-1.40(0.11)$ V, and $-0.18(0.20)$ V, and $+0.39(0.04)$ V (*vs.* SCE). Because of this poly-methylene chain, the reductive

potentials are shifted, compared to **3**, due to the low lying electrons from the ester and carbonyl groups. Comparatively the ΔE_p values are higher, this is due to the the polymethylene linking chain, and as the larger the chain gets the larger the ΔE_p values get. This is indicative of a lesser stability and much slower electron transfers.

Complex **5**, which has a **bqp** ligand chelated to the cobalt instead of **tpy**, was investigated using cyclic voltammetry. Figure 14 shows a representative voltammogram.

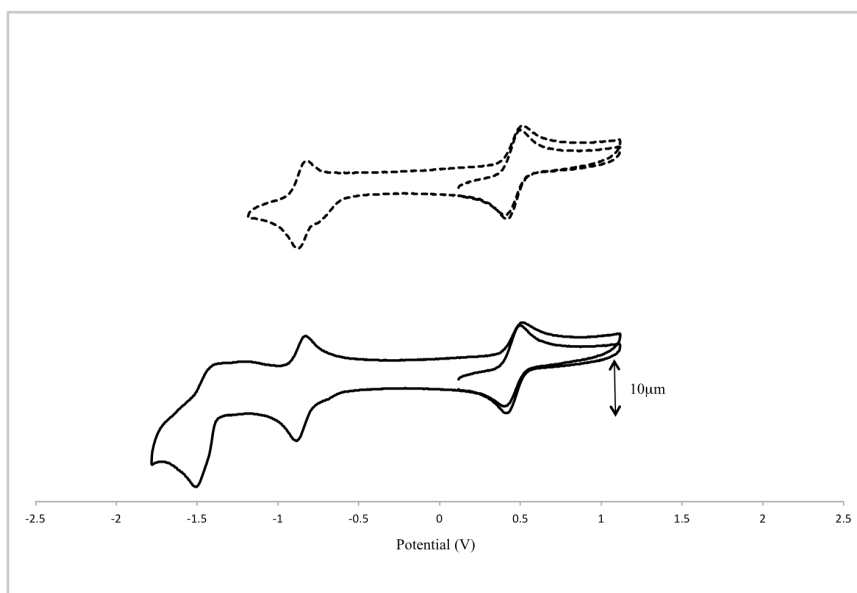


Figure 15: Selected voltammogram for the oxidation and second reduction of $[\text{Co}(\text{mer-}\mathbf{bqp}\text{-}\kappa^3\text{N},\text{N}',\text{N}'')(\mathbf{bpy}\text{-}\kappa^2\text{N},\text{N}')\text{Cl}][\text{Br}_3]_2$ in acetonitrile-TBAPF₆ media. Top; Oxidation with first reduction, Bottom; Oxidation with second reduction.

This voltammogram shows four redox processes for **5** with $E_{1/2}$ (ΔE_p) redox potentials at -1.93 V, -1.50 V, -0.86 V (25.0 mV), and +0.45 V (30.0 mV) (vs. SCE). Based on similar structural characteristics, these redox processes are assigned in analogy to complexes **3** and **4** as ligand-based ($\mathbf{bqp}^{0/-}$), $\text{Co}^{\text{I/II}}$, $\text{Co}^{\text{II/III}}$, and $\text{Co}^{\text{III/IV}}$ couples, respectively^{41,42}. Relative to complexes **3** and **4**, complex **5** shows its oxidation potential at +0.45 V (30.0 mV) which is a +0.06 V shift in the oxidation potential. This positive shift can be

ascribed to the different geometry about the cobalt center due to the coordination of the **bqp**. The reduction potentials for complex **5** are similar to complexes **3** and **4** but shifted to more reductive values. As seen in Figure 15, the first reduction at -0.86 V is quasi-reversible with a small shoulder peak at which is suggestive of decomposition, and subsequent scanning shows that the complex starts to decompose after the second reduction (Figure 14). Compared to complexes **3** and **4** where the **tpy** ligand is rigid, the **bqp** ligand on complex **5** has an extra methylene unit which allows for extra conformation flexibility. This conformation flexibility appears to result in decomposition of complex **5** based on structural similarity to complexes **3** and **4**.

CHAPTER 4

1. CONCLUSION

Homoleptic, meridionally-coordinated tridentate 2,6-bis(8'-quinolinyl)pyridine (**bqp**) cobalt complexes [Co(*mer*-**bqp**- κ^3N,N',N'')₂][PF₆]₂ (**1**) and [Co(*mer*-**bqp**- κ^3N,N',N'')₂][Br₃]₃ (**2**) have been synthesized and characterized. X-ray diffraction shows that the **bqp** ligand adopts a twisted, near-octahedral arrangement relative to the cobalt center. For cobalt(II), complex **1**, coordination of the **bqp** ligand gives a tetragonally compressed Co-N₆ coordination geometry having pseudo D_{4h} symmetry. Coordination of **bqp** to Co(III), complex **2**, produced two crystallographically independent asymmetric units having O_h symmetry. Magnetic susceptibility measurements revealed that **1** produced an effective magnetic moment of 3.8 BM, consistent with a high-spin configuration. Complex **2** revealed no observable magnetic moment, which is consistent with a low-spin configuration. These results combined with X-ray crystallography data have allowed us to assign the electronic configuration as b₂²g e_g³ b₁¹g a₁¹g and t₂⁶g for complex **1** and **2**, respectively. Electronic spectra display intense π - π^* ligand centered (**bqp**) transitions in the 200–380 nm region and low intensity mixed charge transfer transitions between the 400–550 nm region. The electrochemistry of these compounds has been studied. Cyclic voltammetry measurements have shown that the first oxidation scan for both complex **1** and **2** are reversible with potentials more positive than comparable cobalt-terpyridine complexes. Subsequent reductive sweeps indicate decomposition.

Similarly heteroleptic, meridionally-coordinated tridentate 2,2';6',2''-terpyridine, (**tpy**) and bidentate 2,2-bipyridine (**bpy**) and 1,10-phenanthroline (**phen**) cobalt chloride complexes $[\text{Co}(\textit{mer}\text{-tpy-}\kappa^3N,N',N'')(\text{phen-}\kappa^2N,N')\text{Cl}][\text{PF}_6]_2$ (**3**), $[\text{Co}(\textit{mer}\text{-tpy-}\kappa^3N,N',N'')(\text{bpy-}\kappa^2N,N')\text{Cl}][\text{PF}_6]_2$ (**4**) have been synthesized and characterized. X-ray diffraction of **3** and **4** show that the ligands adopt similar linear bite angles and bond lengths. The x-ray data also showed that along with a chlorine ligand allows these two (**tpy**) complexes to adopt an octahedral arrangement around the cobalt core. Cyclic voltammetry measurements have shown that the first oxidation scan for both complexes **3** and **4** are reversible with potentials more positive than comparable cobalt-terpyridine complexes.⁴⁰ Additionally **3** and **4** show remarkable stability under these harsh conditions similar to previously synthesized complexes⁴⁰.

Complex **5** was prepared using a synthetic method as previously discussed in this thesis. The electrochemical data shows similar redox values relative to previous (**tpy**) complexes, where in the first oxidation scan for complex **5** is reversible with a potential more positive than comparable cobalt-terpyridine complexes. Despite numerous attempts the (**bqp**) complex could not be characterized by x-ray or NMR because it appears to decompose readily in solution, which is proven throughout numerous cyclic voltammetric scans.

In summary, electrochemical data for the homoleptic $[\text{Co}(\textit{mer}\text{-bqp-}\kappa^3N,N',N'')_2]^{n+}$ (where n is 2⁺ or 3⁺) system suggests that it will provide a platform for applications such as redox mediators in dye-sensitized solar cells (DSSCs) and catalysis. Regarding the stability for complexes $[\text{Co}(\textit{mer}\text{-tpy-}\kappa^3N,N',N'')(\text{bpy-}\kappa^2N,N')\text{Cl}]^{2+}$ (**3**) and $[\text{Co}(\textit{mer}\text{-tpy-}$

$\kappa^3N,N',N''(\mathbf{phen}\text{-}\kappa^2N,N')\text{Cl}]^{2+}$ (**4**), further work will focus on the spectrochemical series development, catalysis, and characterization. Concerning similar Co^{3+} complexes incorporating the **bqp** ligand, complex **5**, it appears the conformational flexibility destabilizes ligand coordination to the point of decomposition.

APPENDIX

Supplementary Information: Table of Contents

Table S1. Selected bond length [Å] and angles [°] for [Co(<i>mer</i> -tpy- κ^3N,N',N'') ₂] ²⁺ and [Co(<i>mer</i> -tpy- κ^3N,N',N'') ₂] ³⁺ .	46
Table S2. Density functional Theory Calculations. Selected bond length [Å] and angles [°] for [Co(<i>mer</i> -bqp- κ^3N,N',N'') ₂] ²⁺ (low and high spin) and [Co(<i>mer</i> -bqp- κ^3N,N',N'') ₂] ³⁺ .	47
Table S3-A. Optimized Geometry of Co(<i>mer</i> -bqp- κ^3N,N',N'') ₂ ²⁺ (1) in the Doublet Ground State with E(B3LYP) = -2244.39629091 au.	48
Table S3-B. Calculated doublet excited states of for [Co(<i>mer</i> -bqp- κ^3N,N',N'') ₂] ²⁺ (1) in acetonitrile (CH ₃ CN).	50
Table S3-C. Fragment Analysis Based on Mullikan Populations for Co(<i>mer</i> -bqp- κ^3N,N',N'') ₂ ²⁺ (1) in the Doublet Ground State (Alpha-Spin).	54
Table S3-D. Fragment Analysis Based on Mullikan Populations for [Co(<i>mer</i> -bqp- κ^3N,N',N'') ₂] ²⁺ (1) in the Doublet Ground State (Beta-Spin).	56
Table S4-A. Optimized Geometry of [Co(<i>mer</i> -bqp- κ^3N,N',N'') ₂] ³⁺ (2) in the Singlet Ground State with E(B3LYP) = -2244.20766539 au.	58
Table S4-B. Calculated singlet excited states of for [Co(<i>mer</i> -bqp- κ^3N,N',N'') ₂] ³⁺ (2) in acetonitrile (CH ₃ CN).	60
Table S3-C. Calculated triplet excited states of for [Co(<i>mer</i> -bqp- κ^3N,N',N'') ₂] ³⁺ (2) in acetonitrile (CH ₃ CN).	63
Table S4-D. Fragment Analysis Based on Mullikan Populations for [Co(<i>mer</i> -bqp- κ^3N,N',N'') ₂] ³⁺ (2) in the Singlet Ground State.	64
Figure S1. Cobalt-Bis(8'-quinoliny)pyridine (bqp) Geometries	66
Figure S2. Cobalt-Bis(8'-quinoliny)pyridine (bqp) Configurations.	67
Figure S3. Overlay of the x-ray structures at 100 and 290 K for the dication of [Co(<i>mer</i> -bqp- κ^3N,N',N'') ₂].	68

Table S1. Selected bond length [Å] and angles [°] for [Co(*mer-tpy-κ³N,N',N'')₂]²⁺ and [Co(*mer-tpy-κ³N,N',N'')₂]³⁺.**

[Co(<i>mer-tpy-κ³N,N',N'')₂]²⁺</i>			
Co1–N2G	2.0827	Co1–N2B	2.0827
Co1–N1E	1.9131	Co1–N1	1.9131
Co1–N2E	2.0827	Co1–N2	2.0827
N2G–Co1–N1E	79.40	N1–Co1–N2B	79.40
N2E–Co1–N1E	79.40	N1–Co1–N2	79.40
N2G–Co1–N2E	158.81	N2B–Co1–N2	158.81
N1–Co1–N2B	79.40	N1–Co1–N2E	100.6
N1–Co1–N2	79.40	N1–Co1–N2G	100.6
N1–Co1–N1E	180.0	N1E–Co1–N2G	79.40
N1–Co1–N2E	91.94	N1E–Co1–N2E	79.40
N1–Co1–N2G	100.3		
[Co(<i>mer-tpy-κ³N,N',N'')₂]³⁺</i>			
Co1–N2	1.9310	Co1–N5	1.9360
Co1–N1	1.8639	Co1–N4	1.8531
Co1–N3	1.9260	Co1–N6	1.9200
N1–Co1–N2	81.71	N4–Co1–N5	82.42
N1–Co1–N3	82.54	N4–Co1–N6	82.05
N2–Co1–N3	164.45	N5–Co1–N6	164.45
N1–Co1–N5	98.44	N4–Co1–N6	82.05
N1–Co1–N6	97.11	N4–Co1–N5	82.42
N1–Co1–N4	178.94	N5–Co1–N3	90.79
N2–Co2–N4	97.68	N5–Co1–N2	90.36
N3–Co2–N4	98.09		

Table S2. Density functional Theory Calculations. Selected bond length [Å] and angles [°] for $[\text{Co}(\text{mer-bqp-}\kappa^3\text{N,N',N''})_2]^{2+}$ (low and high spin) and $[\text{Co}(\text{mer-bqp-}\kappa^3\text{N,N',N''})_2]^{3+}$.

$[\text{Co}(\text{mer-bqp-}\kappa^3\text{N,N',N''})_2]^{2+}$ (high spin)		$E(\text{UB3LYP}) = -2244.39629091$	
Co1-N1	2.07659	Co1-N4	2.17752
Co1-N2	1.93879	Co1-N5	1.95214
Co1-N3	2.07545	Co1-N6	2.18147
N2-Co1-N1	89.230	N5-Co1-N4	87.911
N2-Co1-N3	89.359	N5-Co1-N6	87.834
N1-Co1-N3	178.574	N4-Co1-N6	175.736
N2-Co1-N4	92.134	N5-Co1-N3	90.761
N2-Co1-N6	92.122	N5-Co1-N1	90.651
N2-Co1-N5	179.876		
N2-C9-C8-C7	37.842	N5-C13-C14-C15	39.995
N2-C10-C11-C12	37.349	N5-C16-C17-C18	39.372
$[\text{Co}(\text{mer-bqp-}\kappa^3\text{N,N',N''})_2]^{2+}$ (low spin)		$E(\text{UB3LYP}) = -2244.39629091$	
Co1-N1	2.28678	Co1-N4	2.06268
Co1-N2	2.00604	Co1-N5	1.97632
Co1-N3	2.28504	Co1-N6	2.06262
N2-Co1-N1	87.633	N5-Co1-N4	89.433
N2-Co1-N3	90.524	N5-Co1-N6	89.525
N1-Co1-N3	174.088	N4-Co1-N6	178.946
N2-Co1-N4	90.518	N5-Co1-N3	92.979
N2-Co1-N6	90.524	N5-Co1-N1	92.931
N2-Co1-N5	179.936		
N2-C9-C8-C7	42.233	N5-C13-C14-C15	37.108
N2-C10-C11-C12	41.982	N5-C16-C17-C18	36.970
$[\text{Co}(\text{mer-bqp-}\kappa^3\text{N,N',N''})_2]^{3+}$		$E(\text{B3LYP}) = -2244.20766539$	
Co1-N1	2.00182	Co1-N4	2.00508
Co1-N2	1.98406	Co1-N5	1.98440
Co1-N3	2.00601	Co1-N6	2.00514
N2-Co1-N1	90.322	N5-Co1-N4	90.329
N2-Co1-N3	89.686	N5-Co1-N6	90.328
N1-Co1-N3	179.354	N4-Co1-N6	179.952
N2-Co1-N4	89.656	N5-Co1-N3	89.729
N2-Co1-N6	89.686	N5-Co1-N1	89.633
N2-Co1-N5	179.952		
N2-C9-C8-C7	35.167	N5-C13-C14-C15	35.295
N2-C10-C11-C12	35.360	N5-C16-C17-C18	35.284

Table S3-A. Optimized Geometry of $\text{Co}(\text{mer-bqp-}\kappa^3\text{N,N',N''})_2]^{2+}$ (1) in the Doublet Ground State with $E(\text{B3LYP}) = -2244.39629091$ au.

Co	0.46058126	0.07067321	-0.21784043
N	0.33078503	-0.11569599	2.05763456
C	-0.91691172	0.09776923	2.56357665
C	1.38742565	0.13349207	2.81812667
C	-2.06129533	-0.30264806	1.80073748
C	-1.09658350	0.72040566	3.84014943
C	1.30240316	0.64848229	4.12778689
H	2.35693075	-0.05855896	2.36707326
C	-3.31174568	0.09745618	2.26239772
C	-2.01376821	-1.26284656	0.65413004
C	-2.39938259	1.07000020	4.27731296
C	0.05968315	0.97488936	4.62060467
H	2.20668857	0.81650962	4.70212546
C	-3.48347986	0.79834666	3.47568410
H	-4.19522208	-0.14102078	1.68042563
C	-3.04221095	-2.21865765	0.62698845
N	-1.04250515	-1.25477683	-0.30778584
H	-2.52081050	1.56015697	5.23893271
H	-0.05330745	1.42850244	5.60123836
H	-4.48328078	1.08912964	3.78153772
C	-3.14416245	-3.10577182	-0.43176171
H	-3.75230636	-2.26019214	1.44178284
C	-1.10748655	-2.15861743	-1.33144896
C	-2.18338413	-3.05583600	-1.42811633
H	-3.95756598	-3.82249261	-0.47981853
C	-0.08798319	-2.26084946	-2.42213061
H	-2.25879889	-3.70607270	-2.28908959
C	0.50366432	-1.13413374	-3.07971668
C	0.18009940	-3.52223570	-2.94580685
C	1.18104310	-1.31499978	-4.32779837
N	0.41718399	0.09734924	-2.50231371
C	0.93311696	-3.70946192	-4.12506657
H	-0.20549815	-4.40125903	-2.44106561
C	1.39129925	-2.62301783	-4.83324630
C	1.62933831	-0.15618896	-5.01144858
C	0.84741775	1.15701812	-3.17218476
H	1.11536619	-4.71810735	-4.48153322
H	1.92496617	-2.74808667	-5.77093429
C	1.43127884	1.08608900	-4.45346254
H	2.12707763	-0.26727033	-5.97071314
H	0.74984551	2.11360146	-2.66637583
H	1.74847912	1.99425512	-4.95387187
N	-0.87875155	1.62959256	-0.39276548
C	-0.79378611	2.65933412	0.50440272
C	-1.99439829	1.48350208	-1.10163573
C	0.46339846	2.98219340	1.10142901
C	-1.95274451	3.42705564	0.84181446
C	-3.13764294	2.28405938	-0.92330627
H	-1.99659953	0.67627443	-1.82333279
C	0.46158124	3.88319266	2.16193481
C	1.76328151	2.57481205	0.50082946
C	-1.88952556	4.36347958	1.90499105
C	-3.13332280	3.21771063	0.08723678

H	-4.01103480	2.11345315	-1.54218770
C	-0.70910238	4.54520973	2.58763016
H	1.39090688	4.10479851	2.67465355
C	2.79648731	3.52350275	0.54227855
N	1.94016810	1.37779904	-0.12795475
H	-2.78337716	4.92042003	2.16932781
H	-4.01893956	3.80405798	0.31448417
H	-0.65508036	5.23234613	3.42556353
C	4.03610850	3.22684016	-0.00014281
H	2.61504796	4.49515891	0.98049162
C	3.14625597	1.08972471	-0.69490282
C	4.21503395	1.99492985	-0.60788762
H	4.84895538	3.94390012	0.04949598
C	3.43020952	-0.21081277	-1.36119776
H	5.18453957	1.71918269	-0.99926912
C	2.91769066	-1.45249869	-0.87520169
C	4.39240062	-0.25865633	-2.36552370
C	3.55897565	-2.67529171	-1.25027639
N	1.82849395	-1.46359835	-0.04687216
C	4.93276728	-1.47380514	-2.83580404
H	4.75987279	0.66627442	-2.79587938
C	4.56378109	-2.66302725	-2.25107573
C	3.15839986	-3.86566317	-0.59490990
C	1.49993076	-2.59563295	0.56901436
H	5.67506028	-1.45337146	-3.62689797
H	5.02431606	-3.60117341	-2.54596463
C	2.16644415	-3.81645623	0.35718764
H	3.64606428	-4.80196451	-0.85015320
H	0.65048871	-2.54438652	1.23857553
H	1.85021720	-4.69899413	0.90129874

Table S3-B. Calculated doublet excited states of for [Co(*mer*-bqp- κ^3N,N',N'')₂]²⁺ (1) in acetonitrile (CH₃CN).

# ^a	E _{VER} ^b			<i>f</i> ^c	Assignment; MO# → MO# ^d
	nm	1000 cm ⁻¹	eV		
1	1837.4	5.4	0.67	0.0000	175 → 187α(+49%) 177 → 192β(24%) 175 → 184α(+9%)
2	1623.5	6.2	0.76	0.0000	172 → 187α(+37%) 176 → 192β(19%) 179 → 192β(+11%)
3	1127.2	8.9	1.10	0.0002	182 → 187α(+64%) 182 → 184α(+17%)
4	1124.5	8.9	1.10	0.0000	170 → 187α(+25%) 171 → 192β(19%)
5	741.5	13.5	1.67	0.0000	177 → 195β(+50%)
6	670.5	14.9	1.85	0.0001	176 → 195β(22%) 172 → 187α(+13%) 179 → 195β(+12%)
7	560.5	17.8	2.21	0.0001	170 → 187α(+22%) 171 → 192β(+13%)
8	498.8	20.0	2.49	0.0000	181 → 184α(+17%) 178 → 183α(15%) 181 → 183β(14%) 180 → 183β(11%) 178 → 182β(+11%)
9	495.4	20.2	2.50	0.0001	181 → 183α(+21%) 181 → 182β(16%) 180 → 182β(14%) 178 → 184α(11%)
10	483.7	20.7	2.56	0.0000	179 → 185α(+14%) 180 → 186α(+11%) 179 → 184β(11%) 181 → 185β(+11%) 180 → 185β(11%)
11	482.6	20.7	2.507	0.0009	182 → 185α(+15%) 180 → 185α(+11%) 180 → 184β(11%) 181 → 184β(+11%) 179 → 186α(+10%)
12	478.2	20.9	2.59	0.000	177 → 192β(+24%) 175 → 187α(+21%)
13	460.7	21.7	2.69	0.0024	182 → 183α(+62%)
14	449.0	22.3	2.76	0.0007	182 → 183α(+22%) 176 → 195β(+14%)
15	427.1	23.4	2.90	0.0072	182 → 185α(+78%)
16	422.4	23.7	2.97	0.0003	182 → 184α(+77%) 182 → 187α(16%)
17	405.4	24.7	3.06	0.0003	171 → 195β(+28%) 179 → 195β(+9%)
18	399.6	25.0	3.10	0.0000	182 → 186α(+85%)
19	372.0	26.9	3.33	0.0000	
20	370.9	27.0	3.34	0.0100	180 → 182β(+17%) 177 → 182β(+17%) 181 → 182β(16%) 181 → 183α(+13%)
21	368.3	27.2	3.37	0.0788	181 → 182β(+49%) 181 → 183α(+45%)
22	365.1	27.4	3.40	0.0007	179 → 182β(+14%)

23	363.8	27.5	3.41	0.0011	179 → 182β(+51%) 176 → 182β(10%)
24	362.7	27.6	3.42	0.0369	180 → 182β(+41%) 177 → 182β(+10%)
25	359.5	27.8	3.45	0.0380	180 → 183α(+57%)
26	358.4	27.9	3.46	0.0003	181 → 184β(+12%) 181 → 185α(10%)
27	354.9	28.2	3.49	0.0244	181 → 184α(+44%) 181 → 183β(+20%) 180 → 184α(15%)
28	353.6	28.3	3.51	0.0005	173 → 182β(+12%) 174 → 183α(12%)
29	352.8	28.3	3.51	0.0780	177 → 182β(+27%) 180 → 183α(15%) 180 → 182β(10%) 180 → 184B(10%)
30	352.1	28.4	3.52	0.0004	173 → 183β(+9%) 174 → 184α(9%)
31	350.6	28.5	3.54	0.0006	180 → 183β(+32%) 180 → 184α(16%) 178 → 182β(+10%)
32	349.7	28.6	3.55	0.0504	181 → 184β(+46%) 181 → 185α(+17%) 182 → 188α(10%)
33	346.6	28.8	3.58	0.0976	180 → 184β(+28%) 181 → 185α(22%) 177 → 182β(+12%)
34	346.3	28.9	3.59	0.0042	180 → 184α(+34%) 180 → 183β(+26%) 181 → 184α(+14%)
35	345.2	29.0	3.60	0.0270	182 → 188α(+34%) 181 → 185α(+24%) 180 → 184β(+10%)
36	344.5	29.0	3.6	0.0003	174 → 184β(+17%) 176 → 185α(16%) 175 → 185β(14%) 177 → 186α(+12%)
37	343.8	29.1	3.61	0.0168	179 → 184β(+41%)
38	343.5	29.1	3.61	0.0455	180 → 184β(+13%) 175 → 184β(+11%) 179 → 184β(+10%) 174 → 185β(9%) 177 → 185α(9%)
39	341.2	29.3	3.63	0.1162	180 → 185α(+44%) 182 → 188α(15%)
40	341.1	29.3	3.63	0.0137	181 → 183β(+17%) 179 → 183α(16%)
41	337.2	29.7	3.68	0.0119	179 → 183β(+61%)
42	336.9	29.7	3.68	0.0005	179 → 183α(+53%)
43	334.1	29.9	3.71	0.0008	180 → 185β(+45%) 181 → 185β(+18%)
44	332.7	30.1	3.73	0.0148	182 → 189α(+81%)
45	329.8	30.3	3.76	0.0035	181 → 186α(+50%) 178 → 183α(10%)
46	328.3	30.5	3.78	0.0190	177 → 184β(+66%)
47	327.9	30.5	3.78	0.0128	179 → 184α(+75%)
48	327.5	30.5	3.79	0.0037	177 → 183β(+45%) 181 → 186α(+11%)
49	327.3	30.6	3.79	0.0021	179 → 185α(+25%) 178 → 182β(+14%) 181 → 185β(11%)

50	325.1	30.8	3.81	0.0000	178 → 183 α (+27%) 178 → 182 β (+25%) 181 → 185 β (+14%)
51	322.4	31.0	3.85	0.0021	175 → 183 α (+51%) 178 → 184 α (+10%)
52	321.6	31.1	3.85	0.0006	181 → 187 α (+42%) 176 → 182 β (20%)
53	321.6	31.1	3.86	0.0107	180 → 186 α (+40%) 180 → 185 β (+17%)
54	318.7	31.4	3.89	0.0041	182 → 190 α (+70%)
55	318.6	31.4	3.89	0.0583	178 → 183 β (+51%) 178 → 184 α (+24%) 179 → 185 β (+10%)
56	317.2	31.5	3.91	0.0047	181 → 187 α (+22%)
57	316.7	31.6	3.92	0.0190	179 → 185 β (+47%) 178 → 184 α (10%)
58	316.3	31.6	3.92	0.0002	178 → 184 β (+28%) 179 → 185 α (19%) 180 → 187 α (17%)
59	313.9	31.9	3.95	0.0003	180 → 187 α (+53%) 178 → 185 α (11%) 182 → 190 α (+11%)
60	312.2	32.0	3.97	0.0106	175 → 183 α (+23%) 178 → 184 α (13%)
61	311.8	32.1	3.98	0.0012	178 → 184 β (+20%) 177 → 185 β (17%) 182 → 191 α (14%) 176 → 184 β (+14%) 178 → 185 α (+13%)
62	311.0	32.2	3.99	0.0000	182 → 191 α (+58%) 178 → 185 α (+14%)
63	309.1	32.3	4.01	0.0014	177 → 185 β (+27%) 178 → 185 α (+21%)
64	307.6	32.5	4.03	0.0129	179 → 186 α (+21%) 175 → 185 α (9%)
65	306.4	32.6	4.05	0.0050	177 → 185 β (+25%) 171 → 182 β (11%)
66	304.4	32.8	4.07	0.0140	176 → 183 β (+32%) 178 → 185 β (+28%)
67	304.1	32.9	4.08	0.0083	176 → 183 β (+34%) 179 → 186 α (+14%) 178 → 186 α (+11%)
68	303.5	32.9	4.08	0.0016	176 → 184B(+46%)
69	302.3	33.1	4.10	0.0039	177 → 183 α (+32%) 175 → 182 β (+26%) 176 → 184 α (+10%)
70	301.9	33.1	4.11	0.0425	178 → 185 β (+17%) 178 → 187 α (+10%)
71	300.8	33.2	4.12	0.0286	174 → 182 β (+32%) 176 → 183 α (+30%) 175 → 183 β (+12%) 177 → 184 α (+12%)
72	299.8	33.4	4.14	0.0003	174 → 182 β (+19%) 176 → 183 α (18%) 174 → 183 α (11%)
73	299.3	33.4	4.14	0.0042	177 → 183 α (+16%) 175 → 182 β (14%)
74	298.4	33.5	4.16	0.0070	175 → 185 α (+33%) 178 → 186 α (12%)
75	297.7	33.6	4.17	0.0020	175 → 185 α (+32%) 178 → 186 α (+20%) 178 → 185 β (+11%)

^a # is the state. ^bE_{VER} is the energy of the vertical transition. ^c*f* is the oscillator strength. ^dAssignment; MO# → MO# is the occupied and the virtual orbitals that define the transition. The absolute value of the transition coefficient for each transition is given in parentheses.

Table S3-C. Fragment Analysis Based on Mulliken Populations for [Co(*mer*-bqp- κ^3N,N',N'') $_2$] $^{2+}$ (1) in the Doublet Ground State (Alpha-Spin) a

molecular orbital	E_i , eV	Co												$\Sigma_{orb}^{bqp\#1^{\uparrow}}$	$\Sigma_{orb}^{bqp\#2^{\uparrow}}$
		s	p_x	p_x	p_x	d_{z^2}	d_{xy}	d_{xy}	$d_{z^2-y^2}$	d_{xy}	d_{xy}	d_{xy}	d_{xy}		
170 (O)	-12.81	0.00	0.00	0.00	0.58	0.00	0.03	0.33	46.98	0.70	43.21	8.16			
171 (O)	-12.71	0.00	0.02	0.02	0.00	0.19	1.02	1.35	0.00	0.08	84.36	12.94			
172 (O)	-12.33	0.00	0.00	0.01	0.33	0.42	38.36	29.73	0.35	0.09	12.88	17.84			
173 (O)	-12.14	0.03	0.00	0.00	0.00	0.07	0.65	1.08	0.01	0.00	23.74	74.43			
174 (O)	-12.10	0.00	0.02	0.02	0.10	0.02	2.34	1.45	0.16	0.02	13.29	82.59			
175 (O)	-12.02	0.40	0.00	0.00	0.00	0.00	32.93	42.02	0.06	1.63	6.01	16.96			
176 (O)	-11.94	0.00	0.05	0.06	0.04	0.00	0.00	0.02	0.11	0.00	87.43	12.29			
177 (O)	-11.92	0.02	0.02	0.01	0.00	0.02	0.10	0.11	0.00	0.00	82.12	17.59			
178 (O)	-11.59	0.00	0.01	0.01	0.03	0.01	0.78	0.45	2.99	0.07	6.32	89.31			
179 (O)	-11.44	0.00	0.01	0.01	-0.01	0.03	2.88	2.05	0.72	0.04	90.85	3.43			
180 (O)	-11.24	0.13	0.00	0.00	0.00	1.46	0.91	1.47	0.00	0.02	38.07	57.94			
181 (O)	-11.19	0.03	0.21	0.16	0.00	2.80	0.16	0.08	0.00	0.07	56.04	40.45			
182 (O)	-10.78	0.00	0.04	0.07	0.31	0.00	0.31	0.20	0.70	0.02	2.66	95.69			
HOMO-LUMO gap: 3.505 eV (28268.4 cm^{-1})															
183 (V)	-7.28	0.05	0.14	0.12	0.00	0.01	0.19	0.32	0.03	1.76	4.87	92.52			
184 (V)	-7.17	0.07	0.09	0.08	0.00	0.37	0.33	0.80	0.15	7.52	8.34	82.24			
185 (V)	-7.06	0.00	0.10	0.13	0.22	0.00	0.10	0.05	0.11	0.00	95.14	4.12			
186 (V)	-6.86	0.02	0.29	0.22	0.00	0.10	0.03	0.06	0.03	1.47	86.12	11.65			
187 (V)	-6.64	0.48	0.00	0.00	0.00	1.62	0.14	1.09	0.90	50.06	12.77	32.95			
188 (V)	-6.34	0.00	0.03	0.06	0.15	0.00	0.15	0.13	0.16	0.00	23.79	75.46			
189 (V)	-6.17	0.00	0.05	0.05	0.48	0.00	0.07	0.05	0.14	0.00	72.73	26.43			
190 (V)	-6.06	0.21	0.06	0.05	0.00	0.06	0.13	0.08	0.06	3.84	11.06	84.46			
191 (V)	-5.97	0.13	0.20	0.15	0.00	0.17	0.01	0.01	0.00	0.12	75.50	23.71			
192 (V)	-5.72	0.11	0.09	0.07	0.00	0.01	0.12	0.20	0.02	0.72	35.12	63.53			
193 (V)	-5.68	0.00	0.02	0.01	0.20	0.00	0.00	0.00	0.01	0.00	3.05	96.71			

molecular orbital	E, eV	Co											$bq\alpha, \#1^e$		$bq\alpha, \#2^e$	
		s	p_x	p_y	p_z	d^2	d_{xy}	d_{xz}	d_{yz}	d^2-y^2	d_{xy}	Σ_{occ}	Σ_{virt}			
194 (V)	-5.55	0.00	0.22	0.32	0.05	0.00	0.02	0.01	0.00	0.00	0.00	98.53	0.85			
195 (V)	-5.51	0.03	0.48	0.35	0.00	0.02	0.00	0.01	0.00	0.08	0.08	76.62	22.41			
196 (V)	-4.82	0.00	0.51	0.54	2.18	0.00	0.07	0.04	0.12	0.00	0.00	15.88	80.64			
197 (V)	-4.60	0.00	0.68	0.96	1.01	0.00	0.00	0.00	0.00	0.00	0.00	81.43	15.91			
198 (V)	-4.31	1.56	0.00	0.00	0.00	0.02	0.12	0.13	0.00	0.23	29.08	68.87				
199 (V)	-4.17	0.07	1.32	1.02	0.01	0.15	0.00	0.00	0.00	0.05	68.37	29.01				
200 (V)	-3.87	0.03	53.49	41.58	0.21	0.08	0.00	0.00	0.00	0.07	3.07	1.47				

^eThe orbital occupancy status is given in parenthesis (O = occupied, V = virtual). ^fSum of the percent population for the three nitrogen, twenty-one carbon, and fifteen hydrogen atoms present in the 2,6-bis(8'-quinolinyl)pyridine ($bq\alpha$); $C_{28}H_{15}N_3$ ligand.

Table S3-D. Fragment Analysis Based on Mulliken Populations for [Co(*mer*-bqp- κ^2 N, κ' N') 2] $^{2+}$ (1) in the Doublet Ground State (Beta-Spin).^a

molecular orbital	E, eV	Co										Σ_{total}	Σ_{total}
		s	d_{xy}	d_{xz}	d_{yz}	d_{z^2}	d_{xy}	d_{xz}	d_{yz}	$d_{z^2-y^2}$	d_{xy}		
170 (O)	-12.67	0.04	0.02	0.01	0.00	0.60	0.49	0.82	0.00	0.03	85.11	12.57	
171 (O)	-12.28	0.00	0.00	0.00	0.05	0.00	0.11	0.04	58.59	0.93	11.50	28.78	
172 (O)	-12.14	0.05	0.00	0.00	0.00	0.03	0.18	0.17	0.03	0.02	22.82	76.71	
173 (O)	-12.11	0.00	0.03	0.03	0.10	0.02	1.62	1.76	8.26	0.08	13.21	74.89	
174 (O)	-11.93	0.00	0.05	0.06	0.03	0.01	0.44	0.48	1.08	0.01	85.93	11.93	
175 (O)	-11.92	0.01	0.02	0.01	0.00	0.01	0.01	0.04	0.00	0.00	81.46	18.43	
176 (O)	-11.90	0.00	0.00	0.00	0.17	0.38	34.30	27.26	2.87	0.02	17.97	17.03	
177 (O)	-11.64	0.32	0.00	0.00	0.00	0.03	33.83	43.39	0.09	0.75	6.77	14.84	
178 (O)	-11.54	0.00	0.01	0.02	0.03	0.00	0.25	0.11	7.40	0.14	29.25	62.79	
179 (O)	-11.33	0.00	0.01	0.01	0.02	0.12	11.72	8.27	5.45	0.25	58.88	15.29	
180 (O)	-11.22	0.19	0.01	0.01	0.00	0.06	3.55	4.69	0.02	0.00	16.31	75.17	
181 (O)	-11.15	0.02	0.18	0.14	0.00	0.05	0.00	0.01	0.00	0.00	81.49	18.11	
HOMO-LUMO gap: 3.887 eV (31354.2 cm ⁻¹)													
182 (V)	-7.26	0.00	0.04	0.07	0.31	0.00	0.31	0.20	0.70	0.02	2.66	95.69	
183 (V)	-7.14	0.05	0.14	0.12	0.00	0.01	0.19	0.32	0.03	1.76	4.87	92.52	
184 (V)	-7.05	0.00	0.09	0.12	0.21	0.00	0.16	0.12	0.20	0.00	96.46	2.63	
185 (V)	-6.91	0.05	0.23	0.18	0.00	2.03	0.00	0.03	0.00	0.04	92.67	4.76	
186 (V)	-6.34	0.00	0.03	0.09	0.12	0.00	0.20	0.17	0.20	0.00	20.77	78.40	
187 (V)	-6.18	0.42	0.05	0.03	0.00	0.07	0.12	0.33	0.18	10.65	2.83	85.32	
188 (V)	-6.16	0.00	0.05	0.05	0.45	0.00	0.07	0.06	0.22	0.00	75.61	23.50	
189 (V)	-6.06	0.75	0.06	0.04	0.00	5.93	0.01	0.08	0.00	0.03	83.96	9.15	
190 (V)	-5.77	0.16	0.00	0.00	0.00	0.07	0.16	0.07	0.18	12.73	15.05	71.57	
191 (V)	-5.68	0.00	0.01	0.02	0.20	0.00	0.00	0.00	0.01	0.05	3.09	96.62	
192 (V)	-5.64	0.16	0.06	0.04	0.00	3.87	0.08	0.18	0.65	41.55	20.78	32.63	
193 (V)	-5.54	0.00	0.21	0.33	0.05	0.01	0.02	0.02	0.00	0.00	98.49	0.87	
194 (V)	-5.52	0.22	0.31	0.20	0.00	3.46	0.09	0.01	0.01	1.04	76.45	18.21	

molecular orbital	E, eV	Co										bqg #1 ^b		bqg #2 ^b	
		s	dx ² -y ²	dx ² -z ²	dx ² -y ²	dx ² -z ²	dx ² -y ²	dx ² -z ²	dx ² -y ²	dx ² -z ²	dx ² -y ²	dx ² -z ²	Σ _{used}	Σ _{used}	
195 (V)	-5.02	1.42	1.15	0.89	0.01	57.26	0.40	0.00	0.06	3.17	27.56	8.09			
196 (V)	-4.82	0.00	0.50	0.53	2.07	0.00	0.08	0.05	0.15	0.00	14.80	81.82			
197 (V)	-4.59	0.00	0.69	0.98	0.99	0.00	0.00	0.00	0.00	0.00	82.57	14.75			
198 (V)	-4.29	1.07	-0.01	0.00	0.00	0.31	0.18	0.13	0.01	0.90	20.61	76.80			
199 (V)	-4.08	0.01	8.41	6.55	0.03	6.13	0.06	0.00	0.01	0.32	61.49	16.99			
200 (V)	-3.82	-0.01	45.68	35.47	0.18	3.82	0.03	0.00	0.01	0.49	10.19	4.14			

^aThe orbital occupancy status is given in parenthesis (O = occupied, V = virtual). ^bΣ_{used} of the percent population for the three nitrogen, twenty-one carbon, and fifteen hydrogen atoms present in the 2,6-bis(8'-quinolinyl)pyridine (bqg); C₂₃H₁₅N₃ ligand.

Table S4-A. Optimized Geometry of $[\text{Co}(\text{mer-bqp-}\kappa^3\text{N,N',N'')}_2]^{3+}$ (2) in the Singlet Ground State with $E(\text{B3LYP}) = -2244.20766539$ au.

Co	0.43453240	0.04669393	-0.21899092
N	0.34502246	0.02953793	1.78401804
C	-0.87180888	0.14985410	2.40532566
C	1.46189702	0.18814401	2.49912614
C	-2.06597547	-0.26191344	1.74699915
C	-0.94620044	0.67952804	3.73257133
C	1.46182138	0.56834215	3.84871622
H	2.39930418	0.04409780	1.98077561
C	-3.28134103	0.09675163	2.32507471
C	-2.05493322	-1.22488864	0.61880689
C	-2.21209449	0.98502963	4.29413671
C	0.25969459	0.87581045	4.44565204
H	2.40643810	0.67110272	4.36901415
C	-3.35850657	0.74967317	3.57155147
H	-4.20636486	-0.14636043	1.81514296
C	-3.09151778	-2.16811698	0.58288232
N	-1.05266840	-1.26408749	-0.30810007
H	-2.25353946	1.40938985	5.29218493
H	0.22035866	1.25962821	5.46050335
H	-4.33047941	1.01412522	3.97328918
C	-3.14701243	-3.10613470	-0.43453395
H	-3.83559990	-2.17442133	1.36697926
C	-1.07647700	-2.20564529	-1.29703094
C	-2.14239694	-3.11165156	-1.38785820
H	-3.96067214	-3.82173345	-0.48380605
C	-0.04898886	-2.27221536	-2.36485249
H	-2.18860364	-3.80008230	-2.21987037
C	0.55068416	-1.10286801	-2.91510180
C	0.19276487	-3.48614829	-3.00348609
C	1.15261934	-1.16422034	-4.21192363
N	0.54021769	0.08026974	-2.22106600
C	0.91327353	-3.57105288	-4.21153725
H	-0.19744459	-4.40177683	-2.57419693
C	1.33631784	-2.42271833	-4.83935063
C	1.54220684	0.04748380	-4.82919917
C	0.88081310	1.20889171	-2.84903199
H	1.08135646	-4.54286446	-4.66251270
H	1.81709409	-2.45778687	-5.81178576
C	1.34625679	1.24104415	-4.17121508
H	1.98404990	0.02053126	-5.82051301
H	0.81653415	2.12490394	-2.27884762
H	1.59773552	2.19428158	-4.62029824
N	-0.88871657	1.54124224	-0.40513037
C	-0.81541555	2.61614159	0.44381106
C	-1.98783224	1.36516105	-1.14321452

C	0.42351829	2.98326121	1.04359835
C	-1.98774232	3.38922418	0.71868929
C	-3.12719094	2.17416477	-1.02787722
H	-1.98646866	0.53091378	-1.83054180
C	0.39364686	3.93120315	2.06376529
C	1.72992243	2.56728172	0.47738752
C	-1.95361508	4.37332337	1.73927997
C	-3.14892215	3.14475751	-0.05144754
H	-3.98163873	1.97746376	-1.66409523
C	-0.79065288	4.59642943	2.43907112
H	1.31083394	4.18600955	2.58224028
C	2.76452399	3.51259546	0.51312571
N	1.92039095	1.35844341	-0.12944729
H	-2.85677931	4.93531255	1.95490290
H	-4.04183796	3.73440390	0.13212841
H	-0.76021782	5.31973718	3.24653119
C	4.01103641	3.20406040	-0.00558257
H	2.57762360	4.49335339	0.92701825
C	3.13424012	1.05424365	-0.67654358
C	4.19905218	1.96158700	-0.58771416
H	4.82327140	3.92132778	0.04243172
C	3.42292280	-0.25638833	-1.30806792
H	5.17446231	1.67774094	-0.95679725
C	2.87036908	-1.47413855	-0.81744382
C	4.42191629	-0.34128859	-2.27499493
C	3.51114130	-2.71482229	-1.12987932
N	1.74217770	-1.46364138	-0.03728126
C	4.95958357	-1.57410979	-2.69568730
H	4.81939774	0.56746686	-2.71236232
C	4.55391903	-2.74101630	-2.09084356
C	3.07966892	-3.88115124	-0.45539836
C	1.38686805	-2.57562587	0.61167768
H	5.73007667	-1.58468678	-3.45880711
H	5.01478040	-3.69214036	-2.33781855
C	2.05834170	-3.79776649	0.46438705
H	3.56741296	-4.82794107	-0.66591431
H	0.51709169	-2.51351902	1.25051056
H	1.72003459	-4.65824093	1.02890342

Table S4-B. Calculated singlet excited states of for [Co(*mer*-bqp- κ^3N,N',N'')₂]³⁺ (2) in acetonitrile (CH₃CN).

# ^a	E _{VER} ^b			<i>f</i> ^c	Assignment; MO# → MO# ^d
	nm	1000 cm ⁻¹	eV		
1	527.4	19.0	2.35	0.0004	180 → 182(+47%) 165 → 182(14%) 173 → 182(8%) 162 → 182(+8%) 159 → 182(6%) 155 → 182(6%) 151 → 182(+5%)
2	496.2	20.2	2.50	0.0016	179 → 183(+30%) 160 → 183(+18%) 171 → 183(+11%) 161 → 182(+9%) 152 → 183(+7%) 169 → 183(+6%) 178 → 182(+3%)
3	492.2	20.3	2.52	0.0000	179 → 182(+40%) 161 → 183(+16%) 160 → 182(+11%) 171 → 182(+7%) 152 → 182(+4%) 169 → 182(+4%) 178 → 183(+3%) 167 → 183(+3%) 153 → 183(+2%)
4	488.7	20.5	2.54	0.0000	181 → 182(+99%)
5	449.7	22.2	2.76	0.0003	181 → 183(+92%) 180 → 182(+3%)
6	444.1	22.5	2.79	0.0020	180 → 182(+49%) 165 → 182(+11%) 173 → 182(+9%) 181 → 183(6%) 162 → 182(6%) 151 → 182(5%) 155 → 182(+5%) 159 → 182(+4%)
7	442.0	22.6	2.81	0.0000	180 → 183(+96%)
8	414.6	24.1	2.99	0.0053	178 → 182(+87%) 179 → 183(6%) 161 → 182(+3%)
9	408.9	24.5	3.03	0.0000	179 → 182(+44%) 178 → 183(21%) 161 → 183(20%) 167 → 183(4%) 153 → 183(2%) 161 → 186(2%)
10	385.6	25.9	3.22	0.0401	181 → 184(+98%)
11	375.6	26.6	3.30	0.0097	181 → 185(+72%) 180 → 184(24%)
12	373.3	26.8	3.32	0.0001	178 → 183(+67%) 179 → 182(+8%) 161 → 183(4%) 180 → 185(3%) 171 → 182(3%) 160 → 182(3%) 175 → 182(2%)
13	370.3	27.0	3.35	0.4478	180 → 184(+73%) 181 → 185(+23%)
14	368.2	27.2	3.37	0.0197	179 → 183(+42%) 161 → 182(18%) 176 → 182(+9%) 178 → 182(+6%) 167 → 182(4%) 170 → 182(+3%) 153 → 182(3%)
15	366.4	27.3	3.38	0.0000	177 → 182(+99%)
16	364.9	27.4	3.40	0.0821	180 → 185(+95%) 178 → 183(+3%)
17	363.9	27.5	3.41	0.0109	176 → 182(+89%) 179 → 183(5%) 161 → 182(+2%)

18	355.1	28.2	3.49	0.0385	181 → 186(+87%) 180 → 187(4%) 178 → 184(3%)
19	354.6	28.2	3.50	0.0026	175 → 182(+93%)
20	352.8	28.3	3.51	0.0000	180 → 186(+54%) 181 → 187(35%) 179 → 184(5%) 178 → 185(+3%)
21	346.8	28.8	3.58	0.0050	174 → 182(+90%) 177 → 183(+4%) 180 → 187(3%)
22	343.1	29.1	3.61	0.0000	181 → 187(+56%) 180 → 186(+33%)
23	340.2	29.4	3.64	0.0069	177 → 183(+90%) 180 → 187(+5%) 174 → 182(3%)
24	339.5	29.5	3.65	0.0050	180 → 187(+77%) 181 → 186(+5%) 174 → 182(+5%) 177 → 183(4%) 179 → 185(4%) 178 → 184(+2%)
25	338.8	29.5	3.66	0.0026	176 → 183(+96%)
26	334.3	29.9	3.71	0.0009	175 → 183(+50%) 161 → 182(15%) 179 → 183(7%) 171 → 183(+6%) 167 → 182(4%) 160 → 183(+3%) 170 → 182(+3%) 169 → 183(+2%) 152 → 183(+2%)
27	334.1	29.9	3.71	0.0000	173 → 183(+27%) 165 → 183(+15%) 179 → 184(+12%) 180 → 186(+9%) 162 → 183(8%) 174 → 183(+7%) 159 → 183(+6%) 155 → 183(+5%) 151 → 183(4%)
28	331.4	30.2	3.74	0.0000	179 → 184(+73%) 181 → 187(6%) 178 → 185(5%) 173 → 183(5%) 165 → 183(2%)
29	328.1	30.5	3.78	0.0006	178 → 184(+51%) 179 → 185(38%) 180 → 187(8%) 181 → 186(+2%)
30	327.9	30.5	3.78	0.0005	171 → 182(+24%) 161 → 183(14%) 160 → 182(+13%) 169 → 182(+8%) 179 → 182(7%) 152 → 182(+6%) 167 → 183(3%) 175 → 182(3%) 179 → 187(+3%) 178 → 183(+3%) 170 → 183(+2%)
31	325.3	30.7	3.81	0.0049	175 → 183(+45%) 161 → 182(+10%) 179 → 183(+8%) 171 → 183(7%) 160 → 183(6%) 179 → 186(5%) 169 → 183(3%) 167 → 182(+3%) 152 → 183(2%)
32	325.3	30.7	3.81	0.0026	179 → 185(+54%) 178 → 184(+41%)
33	322.4	31.0	3.85	0.0000	174 → 183(+85%) 173 → 183(5%) 178 → 185(+3%)
34	318.9	31.4	3.89	0.0000	178 → 185(+86%) 179 → 184(+6%) 174 → 183(3%)
35	314.0	31.8	3.95	0.0226	179 → 186(+88%) 171 → 183(3%)
36	310.6	32.2	3.99	0.0005	178 → 186(+85%) 179 → 187(7%)
37	308.9	32.4	4.01	0.0168	179 → 187(+54%) 180 → 188(+27%) 181 → 189(7%) 178 → 186(+4%) 171 → 182(3%)
38	307.1	32.6	4.04	0.0040	181 → 188(+69%) 178 → 187(+18%) 180 → 189(7%)

39	304.0	32.9	4.08	0.0078	177 → 184(+78%) 176 → 186(+7%) 178 → 186(+3%) 180 → 188(2%) 181 → 189(+2%)
40	302.7	33.0	4.10	0.0440	176 → 184(+82%) 177 → 186(+9%) 181 → 192(+2%)
41	301.8	33.1	4.11	0.0088	177 → 185(+35%) 178 → 187(+30%) 181 → 188(9%) 180 → 188(+6%) 176 → 187(+4%) 179 → 187(4%)
42	301.8	33.1	4.11	0.0421	180 → 188(+40%) 179 → 187(28%) 181 → 189(8%) 177 → 185(5%) 177 → 184(+5%) 178 → 187(4%) 178 → 186(3%)
43	299.0	33.4	4.15	0.0024	176 → 185(+64%) 172 → 182(18%) 177 → 187(+7%)
44	298.8	33.5	4.15	0.1861	178 → 187(40%) 177 → 185(+40%) 181 → 188(+8%) 176 → 187(+3%)
45	296.8	33.7	4.18	0.0000	172 → 182(+78%) 176 → 185(+15%)

^a # is the state. ^bE_{VER} is the energy of the vertical transition. ^c*f* is the oscillator strength. ^dAssignment; MO# → MO# is the occupied and the virtual orbitals that define the transition. The absolute value of the transition coefficient for each transition is given in parentheses.

Table S3-C. Calculated triplet excited states of for $[\text{Co}(\text{mer-bqp-}\kappa^3\text{N,N',N''})_2]^{3+}$ (2) in acetonitrile (CH_3CN).

# ^a	E _{VER} ^b			<i>f</i>	Assignment; MO# → MO# ^d
	nm	1000 cm ⁻¹	eV		
1	793.1	12.6	1.56	0.0000	165 → 182(26%)
2	751.2	13.3	1.65	0.0000	160 → 182(+25%) 179 → 182(+19%)
3	732.4	13.7	1.69	0.0000	160 → 183(+22%)
4	599.8	16.7	2.07	0.0000	161 → 182(44%)
5	587.0	17.0	2.11	0.0000	161 → 183(+48%)
6	565.4	17.7	2.19	0.0000	165 → 183(21%)
7	508.7	19.7	2.44	0.0000	181 → 182(+52%)
8	507.2	19.7	2.44	0.0000	181 → 183(+19%)
9	503.9	19.8	2.46	0.0000	181 → 184(+36%) 180 → 185(+31%)
10	503.5	19.9	2.46	0.0000	180 → 184(+34%) 181 → 185(+32%)

^a # is the state. ^bE_{VER} is the energy of the vertical transition. ^c*f* is the oscillator strength. ^dAssignment; MO# → MO# is the occupied and the virtual orbitals that define the transition. The absolute value of the transition coefficient for each transition is given in parentheses.

Table S4-D. Fragment Analysis Based on Mulliken Populations for [Co(*mer*-bqp- κ^2 -N,N',N'' π)]²⁺ (2) in the Singlet Ground State.^a

molecular orbital	E, eV	Co											Σ_{total}	Σ_{total}
		s	p_x	p_x	p_x	d_{z^2}	d_{xy}	d_{xy}	$d_{z^2-y^2}$	d_{xy}	Σ_{total}	Σ_{total}		
170 (O)	-16.25	0.00	0.03	0.04	0.09	0.00	0.43	0.40	1.07	0.01			48.93	49.01
171 (O)	-16.05	0.00	0.04	0.04	0.06	0.03	2.87	1.89	3.69	0.11			45.66	45.60
172 (O)	-15.74	0.04	0.00	0.00	0.00	0.01	2.08	2.64	0.00	0.11			46.35	48.76
173 (O)	-15.71	0.00	0.04	0.03	0.00	0.03	0.00	0.00	0.00	0.01			51.15	48.73
174 (O)	-15.06	0.04	0.00	0.00	0.00	0.03	0.01	0.02	0.00	0.07			49.91	49.91
175 (O)	-15.01	0.00	0.05	0.06	0.09	0.00	0.06	0.04	0.08	0.00			49.85	49.77
176 (O)	-14.93	0.00	0.02	0.03	0.06	0.00	0.00	0.00	0.00	0.00			49.95	49.93
177 (O)	-14.91	0.00	0.02	0.01	0.00	0.01	0.00	0.00	0.00	0.00			49.94	50.03
178 (O)	-14.52	0.00	0.02	0.02	0.05	0.00	0.10	0.09	0.25	0.00			49.15	50.32
179 (O)	-14.47	0.00	0.00	0.00	-0.01	0.01	0.71	0.47	0.90	0.03			49.54	48.36
180 (O)	-14.08	0.16	0.00	0.00	0.00	0.06	0.17	0.26	0.00	0.08			49.17	50.09
181 (O)	-14.03	0.00	0.22	0.17	0.00	0.02	0.00	0.00	0.00	0.01			50.25	49.33
HOMO-LUMO gap: 3.199 eV (25803.7 cm ⁻¹)														
182 (V)	-10.83	0.00	0.04	0.03	0.00	41.00	0.66	0.18	0.26	13.83			21.83	22.17
183 (V)	-10.59	0.05	0.00	0.00	0.00	13.97	0.01	0.58	0.65	39.13			22.95	22.66
184 (V)	-10.26	0.00	0.01	0.01	0.02	0.00	0.30	0.20	0.39	0.01			49.32	49.78
185 (V)	-10.19	0.00	0.14	0.21	0.44	0.00	0.01	0.01	0.03	0.00			49.78	49.37
186 (V)	-10.02	-0.02	0.00	0.00	0.00	1.51	0.26	0.09	0.07	5.03			46.51	46.56
187 (V)	-9.93	0.00	0.43	0.33	0.00	3.01	0.05	0.01	0.02	0.99			47.60	47.55
188 (V)	-9.41	0.00	0.06	0.09	0.18	0.00	0.10	0.09	0.23	0.00			49.21	50.05
189 (V)	-9.25	0.00	0.09	0.10	0.15	0.00	0.02	0.02	0.03	0.00			50.20	49.39
190 (V)	-9.09	0.46	0.00	0.00	0.00	0.04	0.17	0.17	0.00	0.25			48.89	50.01
191 (V)	-8.99	0.00	0.17	0.14	0.00	1.17	0.02	0.01	0.01	0.38			49.75	48.35
192 (V)	-8.70	0.17	0.00	0.00	0.00	0.05	0.08	0.13	0.00	0.08			49.58	49.91
193 (V)	-8.57	0.00	0.13	0.14	0.21	0.00	0.01	0.01	0.01	0.00			50.00	49.49

molecular orbital	E, eV	Co										Σ_{occ}	Σ_{virt}	
		s	p_x	p_y	p_z	d_{z^2}	d_{xy}	d_{xz}	d_{yz}	$d_{x^2-y^2}$	d_{xy}			
194 (V)	-8.50	0.00	0.04	0.06	0.13	0.00	0.00	0.00	0.00	0.00	0.00	0.00	49.63	50.14
195 (V)	-8.39	0.00	0.50	0.39	0.00	0.27	0.00	0.00	0.00	0.00	0.00	0.09	49.42	49.32
196 (V)	-7.68	0.00	0.68	0.74	1.11	0.00	0.08	0.05	0.10	0.00	0.00	0.00	49.01	48.21
197 (V)	-7.56	0.00	0.60	0.95	1.95	0.00	0.01	0.00	0.01	0.00	0.00	0.00	47.84	48.63
198 (V)	-7.20	1.91	0.00	0.00	0.00	0.01	0.10	0.13	0.00	0.03	0.00	0.03	49.13	48.69
199 (V)	-7.02	0.00	0.95	0.75	0.00	0.24	0.00	0.00	0.00	0.00	0.00	0.08	48.77	49.20
200 (V)	-6.52	0.00	51.68	40.77	0.16	0.18	0.00	0.00	0.00	0.00	0.00	0.06	3.57	3.57

^aThe orbital occupancy status is given in parenthesis (O = occupied, V = virtual). ^bSum of the percent population for the three nitrogen, twenty-one carbon, and fifteen hydrogen atoms present in the 2,6-bis(8'-quinolinyl)pyridine (bqp): C₂₃H₁₅N₃ ligand.

Figure S1. Cobalt-Bis(8'-quinolinyl)pyridine (bqp) Geometries.

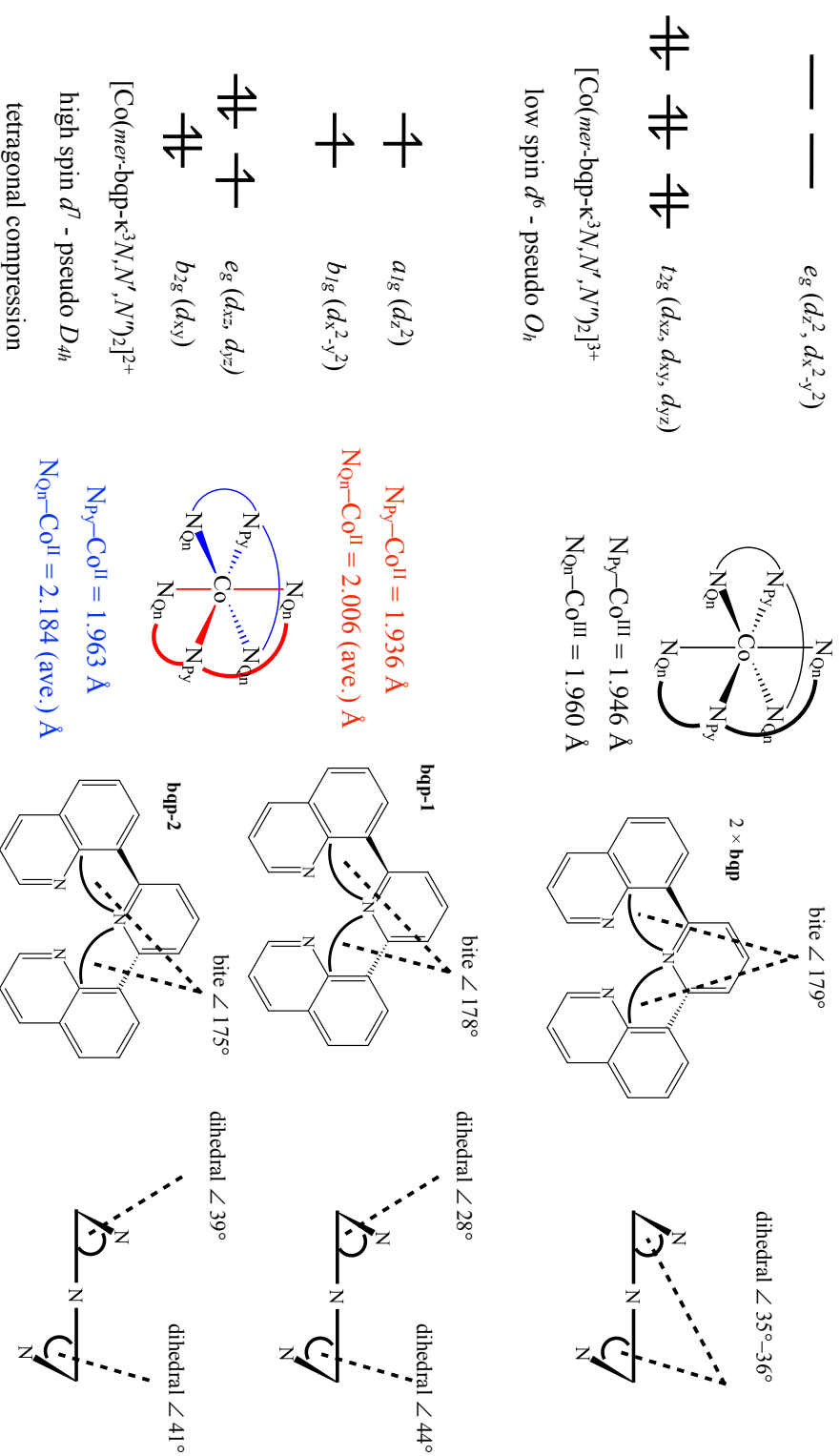


Figure S2. Cobalt-Bis(8'-quinolinyl)pyridine (bqp) Configurations.

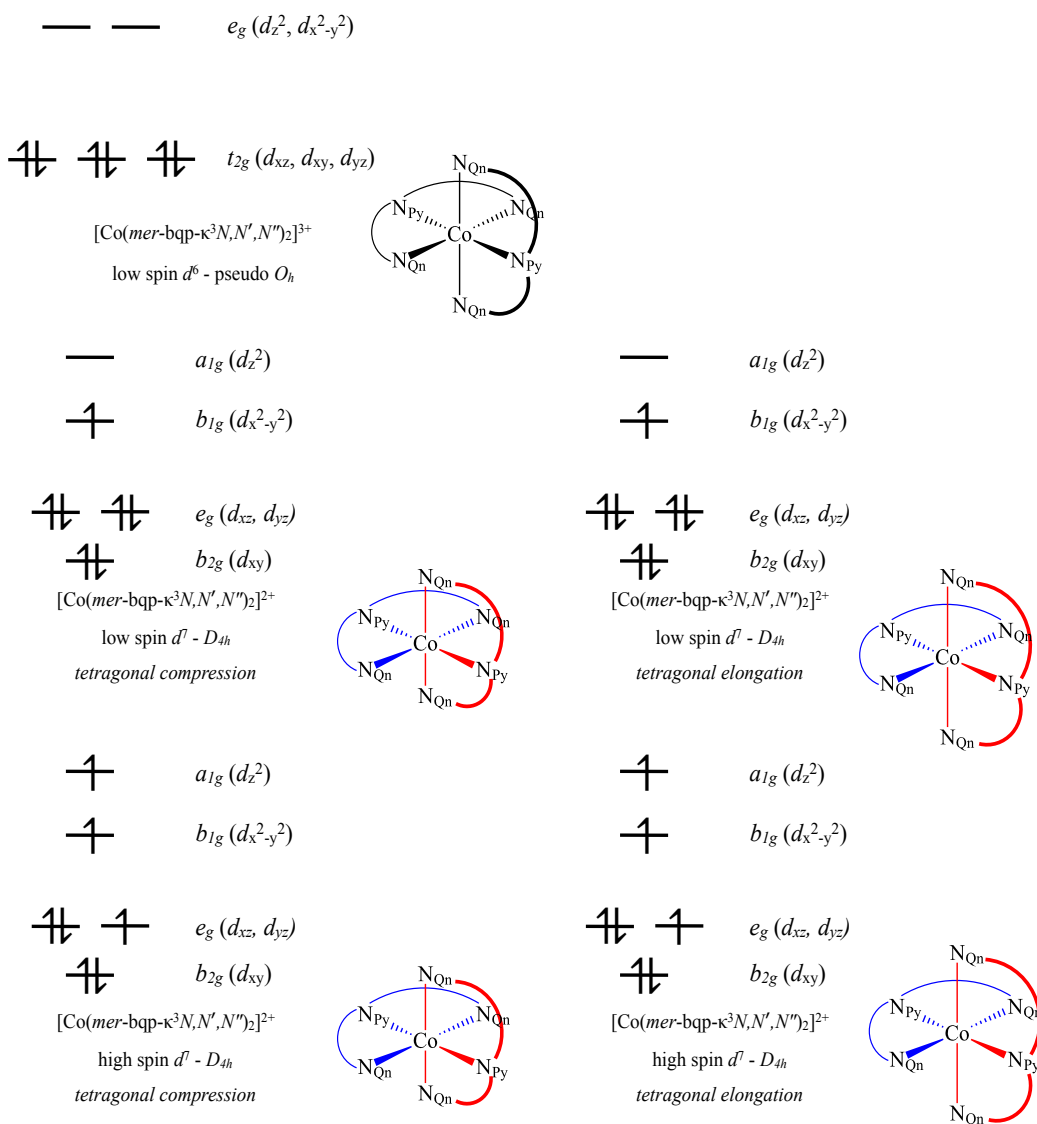
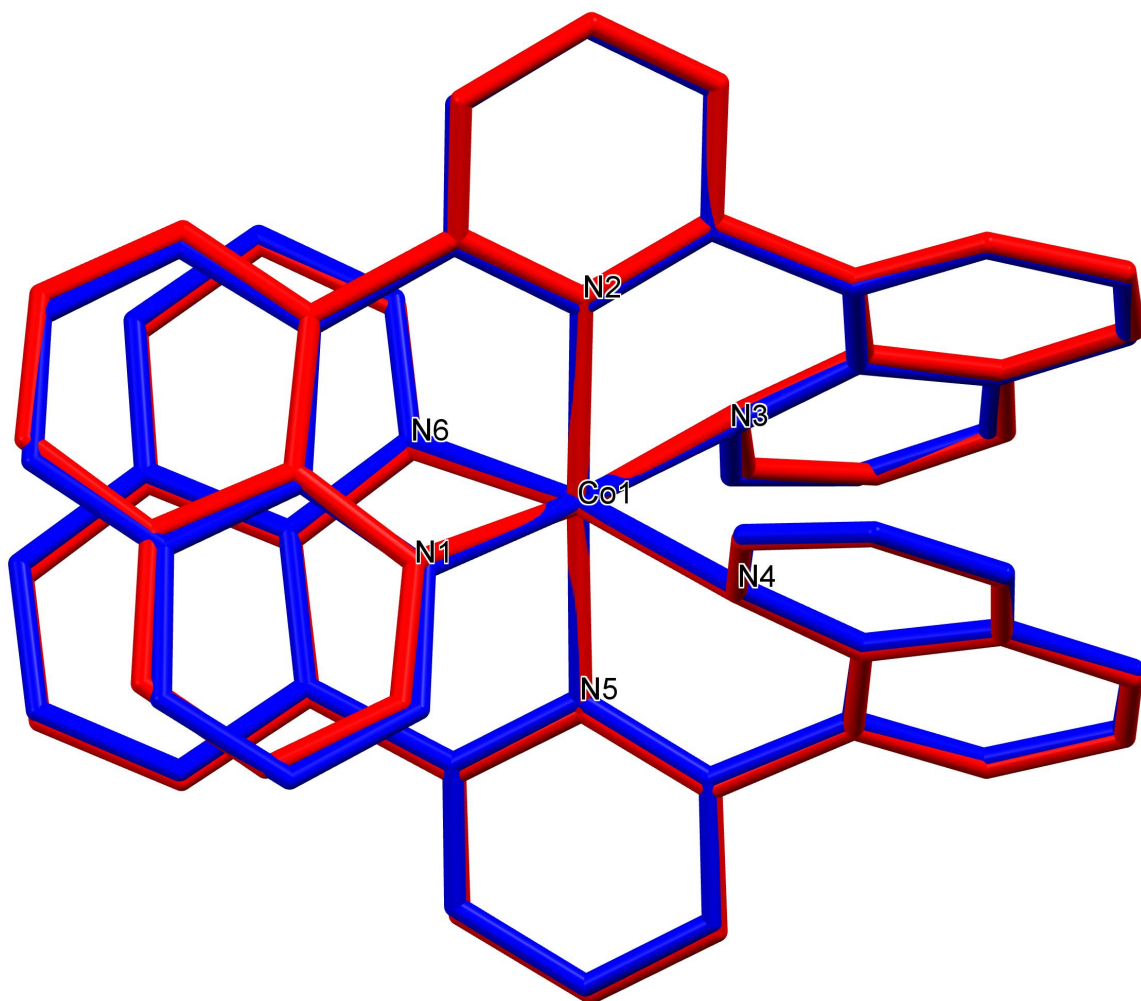


Figure S3. Overlay of the x-ray structures at 100 and 290 K for the dication of $[\text{Co}(\text{mer-bqp-}\kappa^3\text{N,N',N''})_2]$.



REFERENCES:

- [1] Morgan, G.T., Burstall, F.H, *J. Chem. Soc.*, **1932**, 20-30.
- [2] Morgan, G.T., Burstall, F.H, *J. Chem. Soc.*, **1937**, 1649-1655.
- [3] Gratzel, M., *J. Photochem. Photobiol. C*, **2003**, 145-153.
- [4] Eryazici, I., Moorefield, C.N., Newkome, G.R., *Chem. Rev.*, **2008**, 1834-1895.
- [5] a) V. Balzani, J. R. Schoonover and F. Scandola, in *Progress in Inorganic Chemistry: Molecular Level Artificial Photosynthetic Materials*, ed. G. J. Meyer, John Wiley & Sons, Inc., New York, **1997**, vol. 44, ch. 1, pp. 1–96; b) V. Balzani and F. Scandola, in *Supramolecular Photochemistry*, ed., T. J. Kemp, Ellis Horwood, London, **1991**, ch. 2–12, vol. V, pp. 25–394; c) U. S. Schubert, A. Winter and G. R. Newkome, in *Terpyridine-based Materials: Catalytic, Optoelectronic, and Life Sciences Applications*, Wiley-VCH Verlag GmbH & Co., Weinheim, **2011**, ch. 2–4, pp. 13–197; d) L. Flamigni, F. Barigellenti, N. Armaroli, J.-P. Collin, I. M. Dixon, J.-P. Sauvage, J. A. G. Williams, *Coord. Chem. Rev.* **1999**, 190–192, 671–682. e) C. Herrero, B. Lassalle-Kaiser, W. Leibl, A. W. Rutherford, A. Aukauloo, *Coord. Chem. Rev.* **2008**, 252, 456–468. f) M. H. V. Huynh, T. J. Meyer, *Chem. Rev.* **2007**, 107, 5004–5064. g) K. Sakai, H. Ozawa, *Coord. Chem. Rev.* **2007**, 251, 2753–2766. h) G. F. Swiegers, T. J. Malefetse, *Chem. Rev.* **2000**, 100, 3483–3538. i) E. Baranoff, J.-P. Collin, L. Flamigni, J.-P. Sauvage, *Chem. Soc. Rev.* **2004**, 33, 147–155.

- [6] a) U. S. Schubert, A. Winter and G. R. Newkome in *Terpyridine-based Materials: Catalytic, Optoelectronic, and Life Sciences Applications*, Wiley-VCH Verlag GmbH & Co., Weinheim, **2011**, ch. 2–4, pp. 13–197.
- [7] Fallahpour R.A, *Synthesis*, **2003**, 155-184.
- [8] a) M. Beley, C.-A. Bignozzi, G. Kirsch, M. Alebbi and J.-C. Raboin, *Inorg. Chim. Acta* **2001**, **318**, 197–200. b) M. K. Nazeeruddin, P. Péchy, T. Renouard, S. M. Zakeeruddin, R. Humphry-Baker, P. Comte, P. Liska, L. Cevey, E. Costa, V. Shklover, L. Spiccia, G. B. Deacon, C. A. Bignozzi and M. Grätzel, *J. Am. Chem. Soc.* **2001**, **123**, 1613–1624. c) N. D. McDaniel, F. J. Coughlin, L. L. Tinker, and S. Bernhand, *J. Am. Chem. Soc.* **2008**, **130**, 210–217. d) H.-W. Tseng, R. Zong, J. Muckerman and R. P. Thummel, *Inorg. Chem.* **2008**, **47**, 11763–11773.
- [9] a) J. J. Concepcion, J. W. Jurass, J. L. Templeton and T. J. Meyer, *J. Am. Chem. Soc.* **2008**, **130**, 16462–16463. b) S. Masaoka and K. Sakai, *Chem. Lett.* **2009**, **38**, 182–183. c) T. Wada, K. Tsuge and K. Tanaka, *Inorg. Chem.* **2001**, **40**, 329–337. d) P.-W. Du, J. Schneider, P. Jarosz, J.-P. and R. Eisenberg, *J. Am. Chem. Soc.* **2006**, **128**, 7726–7727. e) M. Yagi and K. Narita, *J. Am. Chem. Soc.* **2004**, **126**, 8084–8085.
- [10] a) C. Förster, K. Mack, L. M. Carrella, V. Ksenofontov, E. Rentschler and K. Heinze, *Polyhedron*, **2013**, **52**, 576–581. b) Y. Komatsu, K. Kato, Y. Yamamoto, H. Kamihata, Y.H. Lee, A. Fuyuhiko, S. Kawata and S. Hayami, *Eur. J. Inorg. Chem.* **2012**, **16**, 2769–2775. c) S. Hayami, D. Urakami, Y. Kojima, H. Yoshizaki, Y. Yamamoto, K. Kato, A. Fuyuhiko, S. Kawata and K. Inoue, *Inorg. Chem.* **2010**, **49**, 1428–1432. d) P. Nielsen, H. Toftlund, A. D. Bond, J. F. Boas, J. R. Pilbrow, G. R.

- Hanson, C. Noble, M. J. Riley, S. M. Neville, B. Moubaraki, and K. S. Murray, *Inorg. Chem.* **2009**, *48*, 7033–7047. e) S. Hayami, K. Murata, D. Urakami, Y. Kojima, M. Akita and K. Inoue, *Chem. Commun.* **2008**, *44*, 6510–6512. f) A. Galet, A. B. Gaspar, M. C. Muñoz and J. A. Real, *Inorg. Chem.* **2006**, *45*, 4413–4322. g) S. Hayami, R. Moriyama, Y. Shigeyoshi, R. Kawajiri, T. Mitani, M. Akita, K. Inoue and Y. Maeda, *Inorg. Chem.* **2005**, *44*, 7295–7297. h) S. Hayami, Y. Shigeyoshi, M. Akita, K. Inoue, K. Kato, K. Osaka, M. Takata, R. Kawajiri, T. Mitani and Y. Maeda, *Angew. Chem., Int. Ed.* **2005**, *44*, 4899–4903. i) A. B. Gaspar, M. C. Muñoz, V. Niel and J. A. Real, *Inorg. Chem.* **2001**, *40*, 9–10.
- [11] a) A. Breivogel, C. Förster and K. Heinze, *Inorg. Chem.* **2010**, *49*, 7052–7056. b) K. Mack, A. Wunsche von Leupoldt, C. Förster, M. Ezhevskaya, D. Hinderberger, K. W. Klinkhammer and K. Heinze, *Inorg. Chem.* **2012**, *51*, 7851–7858. c) L. Hammarström and O. Johansson, *Coord. Chem. Rev.* **2010**, *254*, 2546–2559.
- [12] Abrahamsson, M. Jäger, R. J. Kumar, T. Österman, P. Persson, H.-C. Becker, O. Johansson and L. Hammarström, *J. Am. Chem. Soc.* **2008**, *130*, 15533–15542.
- [13] T. Nagata and H. Kon, *Inorg. Chem.*, **2009**, *48*, 8593–8602.
- [14] W. L. F. Armarego and C. L. L. Chai, in *Purification of Laboratory Chemicals*, Butterworth-Heinemann, Burlington, 6th edn, **2009**, ch. 4, pp. 91–92.
- [15] N. G. Tsierkezos, *J. Solut. Chem.* **2007**, *36*, 289–302.
- [16] N. G. Connelly and W. E. Geiger, *Chem. Rev.* **1996**, *96*, 877–922.

- [17] M. J. Frisch, G. W. Trucks, H. B. Schlegel, G. E. Scuseria, M. A. Robb, J. R. Cheeseman, G. Scalmani, V. Barone, B. Mennucci, G. A. Petersson, H. Nakatsuji, M. Caricato, X. Li, H. P. Hratchian, A. F. Izmaylov, J. Bloino, G. Zheng, J. L. Sonnenberg, M. Hada, M. Ehara, K. Toyota, R. Fukuda, J. Hasegawa, M. Ishida, T. Nakajima, Y. Honda, O. Kitao, H. Nakai, T. Vreven, J. A. Montgomery, Jr., J. E. Peralta, F. Ogliaro, M. Bearpark, J. J. Heyd, E. Brothers, K. N. Kudin, V. N. Staroverov, R. Kobayashi, J. Normand, K. Raghavachari, A. Rendell, J. C. Burant, S. S. Iyengar, J. Tomasi, M. Cossi, N. Rega, J. M. Millam, M. Klene, J. E. Knox, J. B. Cross, V. Bakken, C. Adamo, J. Jaramillo, R. Gomperts, R. E. Stratmann, O. Yazyev, A. J. Austin, R. Cammi, C. Pomelli, J. W. Ochterski, R. L. Martin, K. Morokuma, V. G. Zakrzewski, G. A. Voth, P. Salvador, J. J. Dannenberg, S. Dapprich, A. D. Daniels, Ö. Farkas, J. B. Foresman, J. V. Ortiz, J. Cioslowski and D. J. Fox, GAUSSIAN 09, (Revision A.02), Gaussian, Inc., Wallingford, CT, **2009**.
- [18] a) C. Lee, W. Yang and R. G. Parr, *Phys. Rev. B: Condens. Matter* **1988**, *37*, 785–789. b) A. D. Becke, *J. Chem. Phys.* **1993**, *98*, 5648–5642.
- [19] a) P. J. Hay and W. R. Wadt, *J. Chem. Phys.* **1985**, *82*, 270–283. b) P. J. Hay and W. R. Wadt, *J. Chem. Phys.* **1985**, *82*, 284–298. c) P. J. Hay and W. R. Wadt, *J. Chem. Phys.* **1985**, *82*, 299–310.
- [20] a) P. C. Hariharan and J. A. Pople, *Mol. Phys.* **1974**, *27*, 209–214. b) C. Jamorski, M. E. Casida and D. R. Salahub, *J. Chem. Phys.* **1996**, *104*, 5134–5147. c) M. Petersilka, U. J. Grossmann and E. K. U. Gross, *Phys. Rev. Lett.* **1996**, *76*, 1212–1215. d) R.

- Bauernschmitt, R. Ahlrichs, F. H. Hennrich and M. M. Kappes, *J. Am. Chem. Soc.* **1998**, *120*, 5052–5059. e) M. E. Casida, *J. Chem. Phys.* **1998**, *108*, 4439–4449.
- [21] R. E. Stratmann, G. E. Scuseria and M. J. Frisch, *J. Chem. Phys.* **1998**, *109*, 8218–8224.
- [22] M. Cossi, N. Rega, G. Scalmani and V. J. Barone, *Comput. Chem.* **2003**, *24*, 669–681.
- [23] G. M. Sheldrick, SHELXL-97, *Program for the Refinement of Crystal Structures*, University of Göttingen, Göttingen, Germany, **997**.
- [24] T. E. Barder, S. D. Walker, J. R. Martinelli and S. L. Buchwald, *J. Am. Chem. Soc.* **2005**, *127*, 4685–4696.
- [25] M. Jäger, L. Eriksson, J. Bergquist and O. Johansson, *J. Org. Chem.* **2007**, *72*, 10227–10230.
- [26] E. C. Constable, T. Kulke, M. Neuburger and M. Zehnder, *New J. Chem.*, **1997**, *21*, 1091–1102.
- [27] A. T. Baker, D. C. Craig and P. Singh, *Aust. J. Chem.*, **1991**, *44*, 1659–1667.
- [28] P. E. Figgins and D. H. Busch, *J. Phys. Chem.*, **1961**, *65*, 2236–2240.
- [29] a) S. Hayami, Y. Komatsu, T. Shimizu, H. Kamihata and Y. H. Lee, *Coord. Chem. Rev.* **2011**, *255*, 1981–1990. b) I. Krivokapic M. Zerara, M. L. Daku A. Vargas, C. Enachescu, C. Ambrus, P. Tregenna-Piggott, N. Amstutz, E. Krausz and A. Hauser, *Coord. Chem. Rev.* **2007**, *251*, 364–378.

- [30] G. Berggren, P. Huang, L. Eriksson, M.F. Anderlund, *Appl. Magn. Reson.*, **2009**, 9-24.
- [31] (a) E.W. Schubert, *J. Chem. Educ.*, **1992**, 62. (b) D.F. Evans, *J. Chem. Soc.*, **1959**, 2003-2005.
- [32] (a) J. Chambers, B. Eaves, D. Parker, R. Claxton, P.S. Ray, S.J. Slattery, *Inorg. Chim. Acta*, **2006**, 2400-2406. (b) B.N. Figgis, Ligand field theory, in: G. Wilkinson (Ed.), *Comprehensive Coordination Chemistry*, vol. 1, Pergamon Press, Oxford, 1987 (Chapter 6).
- [33] (a) S. Arounagiri, D. Easwaramoorthy, A. Ashokkumar, A. Dattagupta, B. G. Maiya, *Proc. Indian Acad. Sci. (Chem. Sci.)* **2000**, *112*, 1-17. (b) A. J. Bard, *J. Am. Chem. Soc.* **1989**, *111*, 8901-8911.
- [34] (a) B. A. Frenzel, J. E. Schumaker, D. R. Black and S. E. Hightower, *Dalton Trans.* **2013**, *42*, 12440-12451. (b) B. A. Frenzel, E. M. Nagel and S. E. Hightower, *Artificial Photosynthesis* **2013**, *1*, 16-23. (c) H. C. Zhao, J. P. Harney, Y.-T. Huang, J.-H. Yum, M. K. Nazeeruddin, M. Grätzel, M.-K. Tsia and J. Rochford, *Inorg. Chem.* **2011**, *51*, 1-3. (d) A. Cannizzo, A. M. Blanco-Rodríguez, A. E. Nahhas, J. Sebera, S. Zális, A. Vlcek Jr. and M. Chergui, *J. Am. Chem. Soc.* **2008**, *130*, 8967-8974. (e) A. Vlcek Jr. and S. Zális, *Coord. Chem. Rev.* **2007**, *251*, 258-287. (f) S. E. Hightower, R. C. Corcoran and B. P. Sullivan, *Inorg. Chem.* **2005**, *44*, 9601-9603. (g) L. Yang, A.-M. Ren, J.-K. Feng, X.-J. Liu, Y.-G. Ma, M. Zhang, X.-D. Lui, J.-C. Shen and H.-X. Zhang, *J. Phys. Chem. A* **2004**, *108*, 6797-6808. (h) D. M. Dattelbaum, R. L. Martin, J. R. Schoonover and T. J. Meyer, *J. Phys. Chem. A* **2004**, *108*, 3518-3526. (i) D. M.

- Dattelbaum, K. M. Omberg, P. J. Hay, N. L. Gebhart, R. L. Martin, J. R. Schoonover and T. J. Meyer, *J. Phys. Chem. A* **2004**, *108*, 3527–3536. j) L. Yang, A.-M. Ren, J.-K. Feng, X.-D. Liu, Y.-G. Ma and H.-X. Zhang, *Inorg. Chem.* **2004**, *43*, 5961–5972.
- [35] S. I. Gorelsky, *SWizard program*, <http://www.sg-chem.net/>, University of Ottawa, Ottawa, Canada, 2010.
- [36] D. Chen, P.-L. Fabre and O. Reynes, *Electrochimica Acta* **2011**, *56*, 8609–8610.
- [37] R.E. Lokhov, *Chem. Heterocycl. Compd.*, **1981**, 72-76.
- [38] E. C. Constable, *Coord. Chem. Rev.* **2008**, *252*, 842–855.
- [39] Zhu, T., Jackson W.G. *Chinese Journal of Inorganic Chemistry*, **2000**, 485-491
- [40] T. Nagata and H. Kon, *Inorg. Chem.*, **2009**, *48*, 8593–8602.
- [41] Papadopoulos, C. D., Hatzidimitriou, A. G., Voutsas, G. P., Lalia-Kantouri, M. *Polyhedron*, **2007**, *26*, 1077–1086.
- [42] Gaudiello, J.G., Bradley, P.G., Norton, K.A., Woodruff, W.H., Bard, A.B. *Inorg. Chem.*, **1984**, *23*, 3–10.